Supporting Information

Mechanism behind oxidase activity of cellulose-active AA10 lytic polysaccharide monooxygenases

Erna K. Wieduwilt,[*a] Marlisa M. Hagemann,[a] Ulf Ryde,[b] and Erik D. Hedegård[*a]

[a] *Department of Physics, Chemistry, and Pharmacy, University of Southern Denmark, Campusvej 55, 5230 Odense, Denmark; E-mail: erdh@sdu.dk; erna@sdu.dk*
[b] *Department of Chemistry, Lund University, Naturvetarvägen 14, 221 00 Lund, Sweden.*

Protein setup for QM/MM calculations

Protein preparation.

The 2.0 Å X-ray crystal structure of *Tf*AA10A (PDB entry 5UIZ) consists of a dimer with a photoreduced copper centre in both chains. Since the active site in chain B is distorted,[1] chain A was used in this study.

The crystal structure (including chain B) consists of 372 amino acids, two copper centres, 264 water molecules, a glycerol molecule (GOL302) and several iodide ions (IOD303 to IOD318), resulting in 3415 non-hydrogen atoms in total. Chain B, the glycerol molecule and the iodide ions were not considered in the calculations. Additionally, three crystal waters (namely WAT402, WAT404 and WAT406) were removed because of their close proximity to protein residues (ASN42, ASN83 and HIS144, respectively) that lead to artificially high van der Waals energies or convergence problems in the equilibration.

In the remaining system, nine amino acids (ASN42, ASN62, CYS70, ASN83, ARG97, MET119, GLN141, ASP168, CYS216) and three water molecules (WAT443, WAT544, WAT553) were modeled with two alternative conformations in the crystal structure. We always kept the conformation with the higher occupancy (there were no conformations with the same occupancy).

Hydrogen atoms were added using the protein preparation tool in Maestro (version 2021-1).[3] The protonation states of all titratable residues (arginine, lysine, histidine, aspartate and glutamate) were examined using the PROPKA software[4] to estimate the pK_a values of the residues, and their solvent exposure and hydrogen bond network were assessed using visual inspection. The structure contained the following titratable residues: 8 arginine, 3 lysine, 10 histidine, 13 aspartate and 3 glutamate. All arginine and lysine residues were protonated ($+1$ charge) and all aspartate and glutamate residues were deprotonated (-1 charge).

The following naming scheme is used to differentiate the three possible protonation states of the histidine residues: histidines with protonation of only $N^{\varepsilon 2}$ or only $N^{\delta 1}$ are labelled HIE and HID, respectively, while histidines protonated at both nitrogens are denoted HIP. The protonation states for the histidines are HIE37, HIP56, HIE58, HIE96, HIP137, HID144, HIP174, HID190, HIE198, HIE208. $N^{\delta 1}$ in HIE37 and $N^{\varepsilon 2}$ in HID144 coordinate the copper ion. $N^{\delta 1}$ in HIE58 is too close to the backbone of HIE58 to be protonated. The proton at $N^{\delta 1}$ in HID199 can form a hydrogen bond with $O^{\gamma 1}$ in THR154. HIE96, HIE198 and HIE208 are buried inside the protein. In HIE198, the proton at $N^{\varepsilon 2}$ can form a hydrogen bond with the backbone oxygen of THR154. HIP56, HIP137 and HIP174 are located on the surface of the protein and solvent-exposed.

The amino-terminal group of nitrogen (HIE37) is doubly protonated and hence neutral. It is part of the histidine brace,[5] which coordinates the copper ion. The C-terminus of VAL222 was modelled as a carboxylate group (charge -1) in the crystal structure, which is clearly supported by the electron density maps, and it was consequently included in the calculations. With the described protonation states and charge assignments, the protein has a total charge of -2.

The protein includes four cysteine residues that are involved in CYS50-CYS70 and CYS106-CYS216 crosslinks, their presence was examined using Maestro. Two different orientations are possible for glutamine, asparagine and histidine residues, which are difficult to distinguish in X-ray data due to the similar scattering power of oxygen and nitrogen. Therefore, their orientation was examined with the protein preparation tool in Maestro and visual inspection of their hydrogen bond network. Residues HIP56, GLN64, ASN83, ASN131, GLN175, ASN184 and ASN193 were flipped compared to their orientation in the crystal structure. Contrary to the suggestion of the protein preparation tool, ASN184 was not flipped because $O^{\delta 1}$ can form a hydrogen bond with $H^{\varepsilon 2}$ in HIP137.

Calculation of RESP charges.

Restrained electrostatic potential (RESP) charges for the subsequent equilibration (see below) were computed for the copper centre and its first coordination sphere (see Fig. S1 left). The input system was extracted from the structures obtained in the setup as described above. Hydrogen atom positions were optimized in Turbomole[6] using TPSS/def2-SV(P) with D3 dispersion correction, Becke-Johnson damping and the resolution of identity (RI) approximation.[7–9]

A development version of Turbomole version 7.5 was used to compute the electrostatic potential in points that were sampled with the Merz-Kollman scheme,[10,11] employing a radius of 2.0 Å for copper[12] and default radii for all other atoms.[11] The RESP charges were calculated by fitting to the obtained electrostatic potential using the resp program in Amber.[13]

Equilibration.

The system obtained after protein setup was equilibrated with Amber[13] using simulated annealing. The system was solvated in an octahedral 20 Å TIP3P water box using tleap (see Fig. S1 middle). Non-hydrogen atoms in the protein and crystal-water oxygen atoms were kept fixed at their crystallographic positions.

The equilibration consisted in a five-step procedure. First the energy of the system was minimized in 1 000 cycles. Second a 10 ps molecular dynamics simulation of 20 000 steps and a time step of 0.0005 ps was performed. Next the system was equilibrated for 1 ns using the SHAKE algorithm to keep bonds involving hydrogen atoms fixed to the equilibrium value, and a time step of 0.002 ps. The volume was kept constant in these three steps.

In the two final steps of the equilibration procedure, the pressure was kept constant and the SHAKE algorithm was applied. During 10 ns of simulated annealing with a time step of 0.002 ps the system was in the fourth step heated to 370 K in the first 3.2 ns, followed

by 6.8 ns of cooling to 0 K. The temperature was regulated using Langevin dynamics with a varying time constant during the simulation: It was set to 0.2 ps in the first 4 ns, 1.0 ps in the following 2.4 ns, 0.5 ps in the next 1.6 ns and 0.05 ps in the final 2 ns. In the fifth and last step of the equilibration procedure, the system was minimized in 10 000 cycles.

For the following QM/MM calculations, a 40 Å sphere was cut out from the octahedral system (see Fig S1 right).

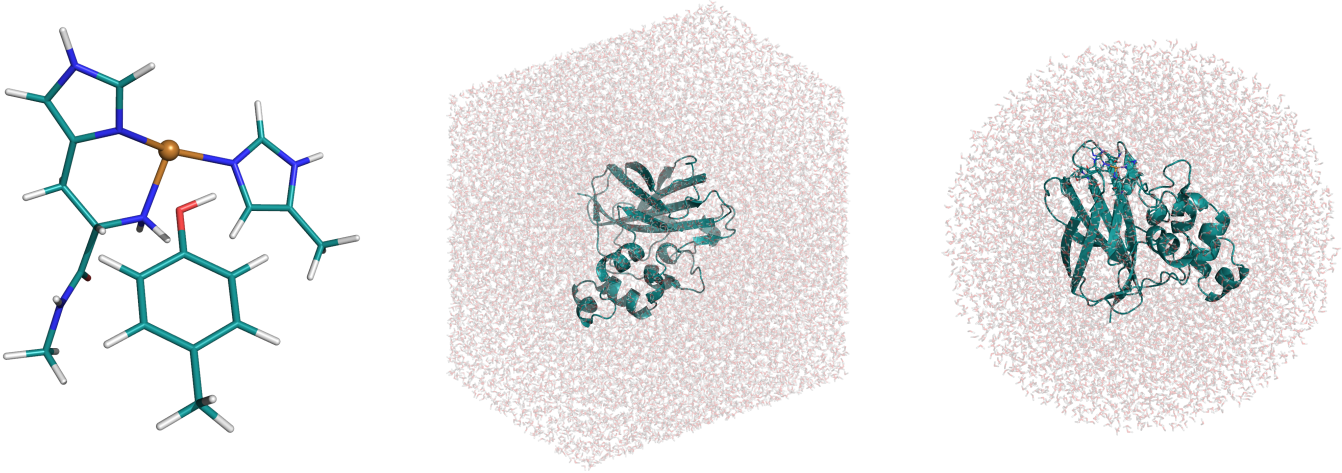

Fig. S1 System used to compute the RESP charges (left), octahedral water box employed in equilibration (middle) and the spherical system used in the QM/MM calculations (right).

QM regions

QM/MM calculations are known to be sensitive to the employed QM region.[14–16] We employed two different QM region sizes in this study, shown in Figure S2. The small QM region consisted of the Cu ion, HIS37 and HIS144 (constituting the histidine brace), HIS208 (used as proton donor), TYR213, GLN211 and ASP140. Additionally, GLY38 (bound to HIS37), ALA142 and SER143 (bound to HIS144), and six water molecules were included in the QM region. Two of the water molecules (W419 and W492) were present in the crystal structure, the remaining water molecules are from the solvation model and are labeled W2 and W4-W6. Since we observed large changes in MM energies of up to 30 kJ/mol with the smaller QM region for some proton-transfer reactions (particularly **3** $\longrightarrow$ **4** and $\mathbf{3}^{red} \longrightarrow \mathbf{4}^{red}$), we mainly show the results for the QM region including two additional water molecules (W1 and W3) and ASP90. In cases where we show results obtained with the small QM region, they are explicitly denoted with the subscript "small".

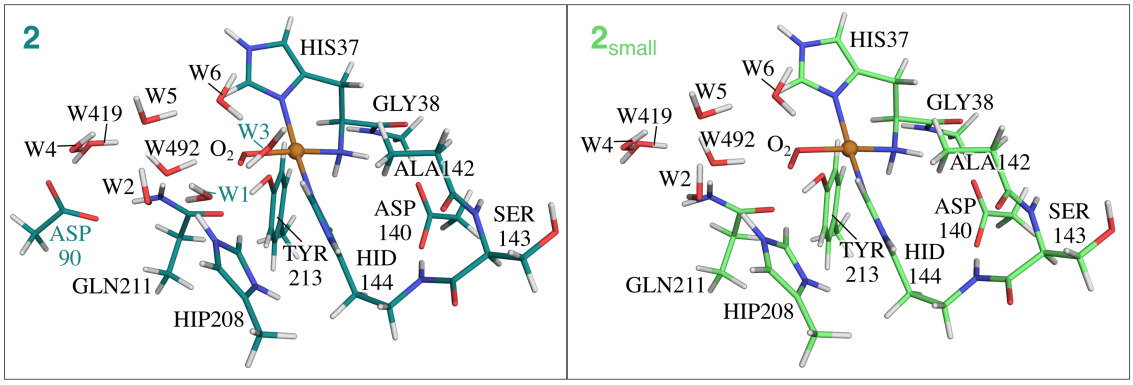

Fig. S2 Smaller and larger QM regions employed in this study. Carbon atoms are shown in light and dark green, and oxygen atoms are shown in light and dark red for the small and large QM regions, respectively.

MM-free calculations

We additionally investigated how optimizing MM residues (optimizing all atoms within 6 Å of any atom in our large QM region) impacts the geometry of several intermediates, in particular: $\mathbf{2a}_{\mathrm{HIP}}$, $\mathbf{3a}_{\mathrm{HIP}}$, $\mathbf{3a}_{\mathrm{HIP}}^{\mathrm{red}}$, $\mathbf{3l}^{\mathrm{red}}$, **4a**, $\mathbf{4a}^{\mathrm{red}}$ and $\mathbf{4f}^{\mathrm{red}}$. We refer to these calculations as MM-free calculations. An overlay of the structures with fixed MM residues is shown in Figure S3.

We note that the geometry changes are small for intermediates $\mathbf{3a}_{\mathrm{HIP}}^{\mathrm{red}}$ (RMSD 0.16), $\mathbf{3l}^{\mathrm{red}}$ (RMSD 0.17), **4a** (RMSD 0.23), $\mathbf{4a}^{\mathrm{red}}$ (RMSD 0.28) and $\mathbf{4f}^{\mathrm{red}}$ (RMSD 0.19).

Larger changes are observed for the superoxide $\mathbf{2a}_{\mathrm{HIP}}$ (RMSD 0.47), where the distance between the distal oxygen atom of the superoxide and the hydrogen atom of HIP increased from 2.63 Å to 3.16 Å, rendering the proton transfer **2a** $\longrightarrow$ **3a** even less likely. QM/MM calculations with optimized MM residues for this proton transfer confirm this: The reaction is uphill (93 kJ/mol for the triplet and 59 kJ/mol for the open-shell singlet) and removing the distant restraint (both for the triplet and the open-shell singlet) leads to the proton transferring back to HIS. This result thus suggests that the observed and discussed differences between TPSS and B3LYP for this particular transfer are geometry dependent (see main text).

Since reaction **2a** $\longrightarrow$ **3a** is unfavorable, the second proton transfer $\mathbf{3a}_{\mathrm{HIP}} \longrightarrow$ **4a** is unlikely to take place. We nevertheless performed MM-free calculations for the reactant and the product. Somewhat larger changes than for the other intermediates are observed for $\mathbf{3a}_{\mathrm{HIP}}$ (RMSD 0.43), where the distance between the proximal oxygen atom of the OOH species and the hydrogen atom of HIP decreased from 3.68 Å to 3.56 Å. However, with TPSS/def2-SV(P) we obtain very similar reaction energies for the reaction $\mathbf{3a}_{\mathrm{HIP}} \longrightarrow$ **4a** with the free and fixed MM regions, namely 5 and 6 kJ/mol, respectively. We thus conclude that the changes to the geometry of $\mathbf{3a}_{\mathrm{HIP}}$ do not change the conclusions drawn for this reaction.

The reaction energy of reaction $\mathbf{3a}_{\mathrm{HIP}}^{\mathrm{red}} \longrightarrow \mathbf{4a}^{\mathrm{red}}$ changes from 19 kJ/mol to 8 kJ/mol when the MM regions for both reactant and product are optimized, showing that this transfer is favorable as we also concluded from calculations with a fixed MM region.

Finally, attempts to obtain $\mathbf{2}_{\mathrm{HIP}}^{\mathrm{red}}$ from MM-free calculations resulted in $\mathbf{3}^{\mathrm{red}}$ (via proton transfer during the optimization as observed before).

Therefore, optimizing the MM residues does not change the main conclusions of this manuscript. This is also in agreement with previous studies, e.g. by Hedegård and Ryde [17].

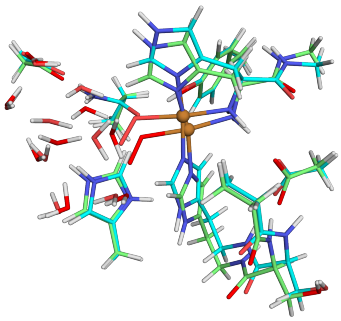

(a) $2a_{HIP}$ (RMSD 0.47)

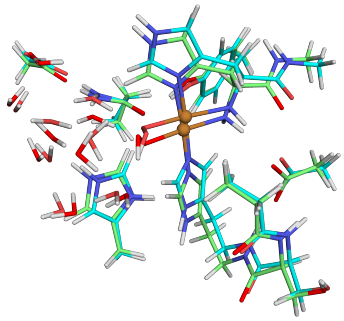

(b) $3a_{HIP}$ (RMSD 0.43)

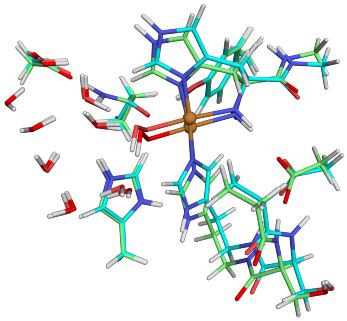

(c) $3a^{red}_{HIP}$ (RMSD 0.16)

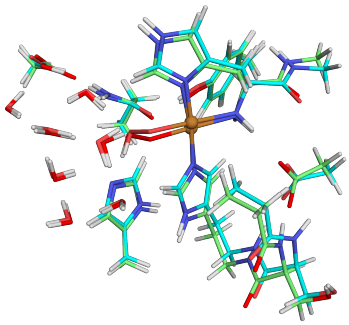

(d) $3l^{red}$ (RMSD 0.17)

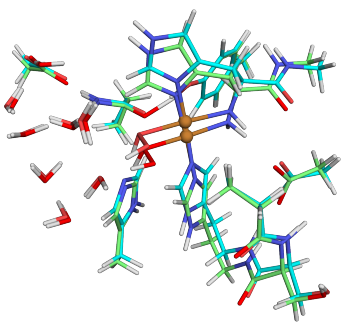

(e) 4a (RMSD 0.23)

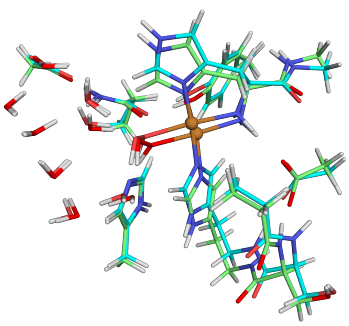

(f) $4a^{red}$ (RMSD 0.28)

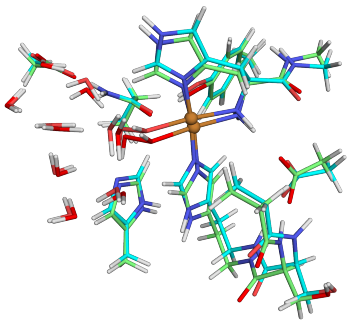

(g) $4f^{red}$ (RMSD 0.19)

Fig. S3 Structure overlay for MM-fixed (light blue carbon atoms) and MM-free (light green carbon atoms) calculations.

The Cu^{+} state 1 and the superoxide state 2

Since *Tf*AA10A is photoreduced in the crystal structure, we started by optimizing the structure with Cu in +I state (intermediate **1**). The QM region consisted of all the protein residues present in the small QM region and WAT492. The optimized structure is shown in Fig. S4. We next added dioxygen to the active site. To allow the hydrogen-bond network to adapt, we moved WAT492 away from the active site into the solvent region, increasing the $Cu{-}O_{WAT492}$ distance from 3.7 Å to 5.2 Å (see Fig. S4). Additionally, we added seven additional water molecules to the QM system (resulting in the QM region shown in Figure 1). The resulting intermediate $\mathbf{2}_{HIE}$ contains a superoxide (see Fig. S4 and Tab. S21) as consistently observed in previous theoretical calculations.[18] Reduction of the superoxide gives intermediate $\mathbf{2}^{red}_{HIE}$ (see Figure S4).

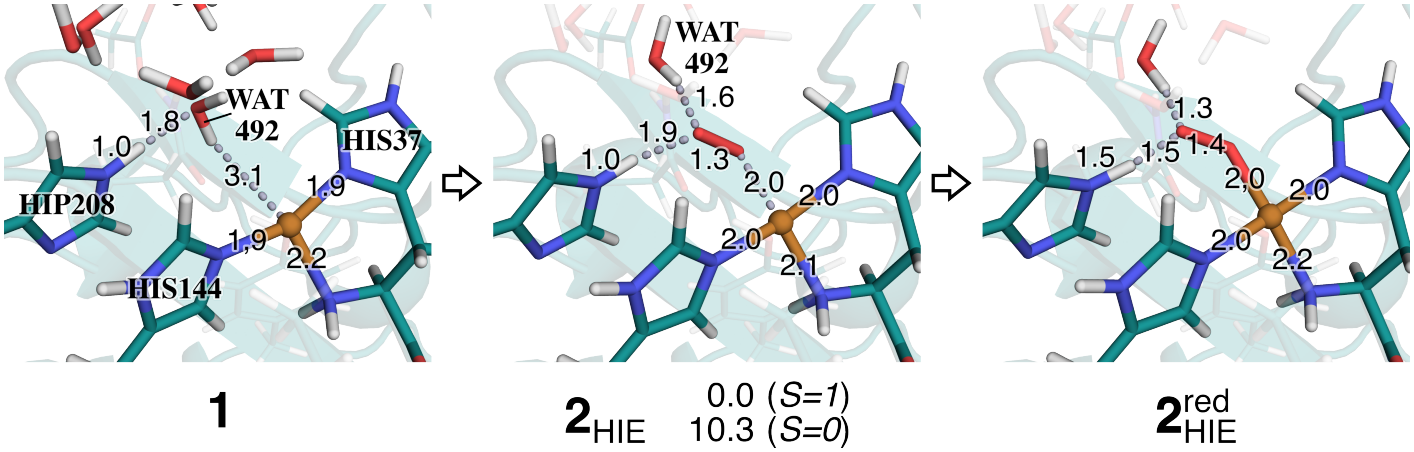

Fig. S4 QM/MM optimized structures of the initial reduced state 1, the superoxide state 2 and the reduced form 2^{red}_{HIE}. Structures were optimized with TPSS/def2-SV(P). Distances are reported in Å. Energies for 2_{HIE} were calculated with B3LYP/def2-TZVPP and are given in kJ/mol with reference to the triplet state.

Table S1 Mulliken spin populations for 2_{HIE}, calculated with def2-TZVPP and surrounding point charges. Only values larger than 0.05 are reported.

Residue	His37		His144	Cu	O_2	
Atom	N	$N^{\delta 1}$	$N^{\varepsilon 2}$	Cu	O^d	O^p
	S=1					
$\mathbf{2}_{HIE}$, TPSS	0.08	0.06	0.07	0.44	0.59	0.69
$\mathbf{2}_{HIE}$, B3LYP	0.08	0.07	0.08	0.51	0.57	0.67
	S=0					
$\mathbf{2}_{HIE}$, TPSS	0.09	0.06	0.08	0.43	−0.40	-0.26
$\mathbf{2}_{HIE}$, B3LYP	-0.09	-0.06	-0.08	-0.54	0.47	0.31

Dissociation

Table S2 Summary of energies for the two types of calculations for dissociation reactions. css stands for closed-shell singlet. Big-QM energies (calculated with B3LYP/def2-SV(P)) are reported in italics for the transfer with a collective variable.

Dissociated species		Spin state	Transfer with collective variable				Interchange of H_2O and oxygen species		Starting structure/
			Reaction barrier	Reaction energy	SI		Reaction energy	SI	
		S	(kJ/mol)	(kJ/mol)	Fig.	Table	(kJ/mol)	Table	Reference
				B3LYP/def2-TZVPP					
2^{dis}	[Cu(II)−$H_2O\cdot O_2^{\cdot-}$]$^+$	*1*	88.7 *100.9*	63.5 *65.3*	S5, S6	S4	85 ± 7 ($n=2$)	S3	**2**$_{HIE}$
		0	89.6 *102.1*	64.8 *66.6*		S6	115 ± 11 ($n=5$)	S5	
	[Cu(I)−$H_2O\cdot O_2$]$^+$	*1*	not observed				56 ± 31 ($n=6$)	S3	
		0	not observed				84 ± 57 ($n=2$)	S5	
3^{dis}	[Cu(II)−$H_2O\cdot OOH^{\cdot}$]$^{2+}$	*1*	proton transfers to HIS208		-	-	-14 ± 21 ($n=7$)	S7	**3**$_{int}$
		0	-	-	-	-	-20 ± 21 ($n=7$)	S8	
	[Cu(III)−$H_2O\cdot OOH^-$]$^{2+}$	css	-	-	-	-	141 ± 38 ($n=7$)	S9	
3^{red,dis}	[Cu(II)−$OH^-\cdot H_2O_2$]$^+$	*1/2*	88.4 *80.3*	29.3 *26.4*	S5, S7	S11	−7 and 37	S10	**3l**^{red}
	[Cu(II)−$H_2O\cdot OOH^-$]$^+$		-	-	-	-	67 ± 16 ($n=3$)		
	+ [Cu(I)−$H_2O\cdot OOH^{\cdot}$]$^+$		-	-	-	-	92 ± 32 ($n=6$)		
4^{red,dis}	[Cu(II)−$H_2O\cdot H_2O_2$]$^{2+}$	*1/2*	66.9 *62.1*	21.3 *26.2*	S5, S8	S13	8 ± 7 ($n=8$)	S12	**4f**^{red}
				TPSS/def2-TZVPP					
2^{dis}	[Cu(II)−$H_2O\cdot O_2^{\cdot-}$]$^+$	*1*	100.9	77.6	S5, S6	S4	67 ± 7 ($n=6$)	S3	**2**$_{HIE}$
		0	104.1	79.1		S6	83 ± 24 ($n=8$)	S5	
	[Cu(I)−$H_2O\cdot O_2$]$^+$	*1*	not observed				43 ± 54 ($n=2$)	S3	
		0	not observed				not observed	S5	
3^{dis}	[Cu(II)−$H_2O\cdot OOH^{\cdot}$]$^{2+}$	*1*	proton transfers to HIS208		-	-	43 ± 23 ($n=7$)	S7	**3**$_{int}$
		0	-	-	-	-	36 ± 23 ($n=7$)	S8	
	[Cu(III)−$H_2O\cdot OOH^-$]$^{2+}$	css	-	-	-	-	92 ± 29 ($n=7$)	S9	
3^{red,dis}	[Cu(II)−$OH^-\cdot H_2O_2$]$^+$	*1/2*	76.9	28.0	S5, S7	S11	−2 and 35	S10	**3l**^{red}
	[Cu(II)−$H_2O\cdot OOH^-$]$^+$		not observed				not observed		
	[Cu(I)−$H_2O\cdot OOH^{\cdot}$]$^+$		not observed				65 ± 24 ($n=6$)		
4^{red,dis}	[Cu(II)−$H_2O\cdot H_2O_2$]$^{2+}$	*1/2*	51.7	20.0	S5, S8	S13	8 ± 8 ($n=8$)	S12	**4f**^{red}

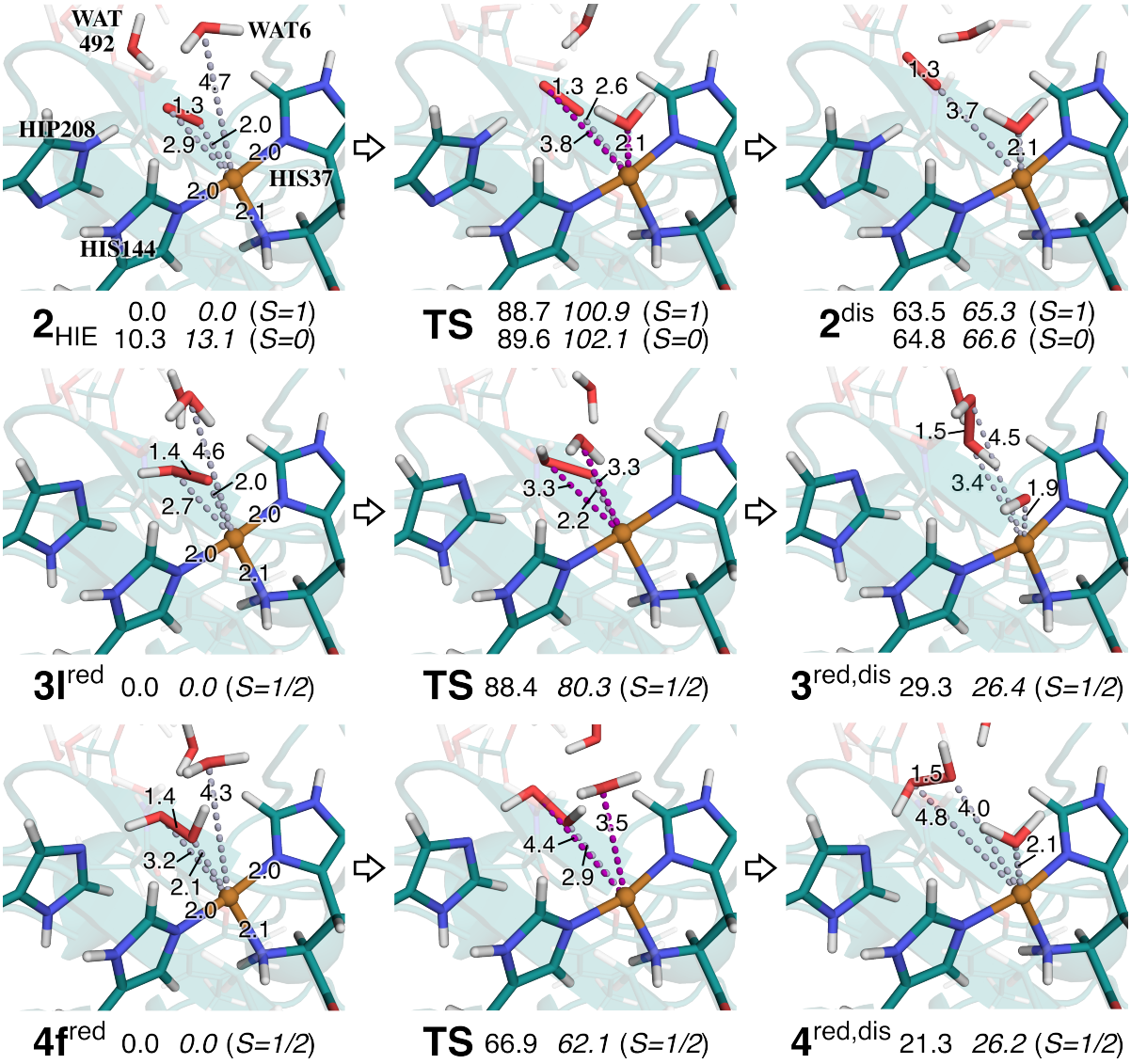

Fig. S5 Reactions $2_{HIE} \longrightarrow 2^{dis}$ (top), $3I^{red} \longrightarrow 3^{red,dis}$ (middle) and $4f^{red} \longrightarrow 4^{red,dis}$ (bottom). Structures were optimized with TPSS/def2-SV(P), and only the most stable electron configuration (triplet or open-shell singlet for the dissociation of superoxide) is shown. Distances are reported in Å and are omitted if they remain constant. Energies were calculated with B3LYP/def2-TZVPP and energies in italics were calculated with B3LYP/def2-SV(P) using the big-QM approach. Energies are reported in kJ/mol relative to 2_{HIP} in the triplet state for the dissociation of superoxide and relative to $3I^{red}$ and $4f^{red}$ for the dissociation of OOH and H_2O_2, respectively.

Table S3 Mulliken spin populations and QM/MM energies for the dissociation of superoxide from 2_{HIE} in triplet spin state, calculated with def2-TZVPP and surrounding point charges. Only atoms for which at least one spin population is greater than 0.05 are listed. Energies are relative to 2_{HIE} in the triplet state.

Residue	His37		His144	Cu	O_2		Distance (Å)		ΔE (kJ/mol)		
Atom	N	$N^{\delta 1}$	$N^{\varepsilon 2}$	Cu	O^1	O^2	$Cu-O^1$	$Cu-O^2$	QM/MM	MM	ptch
	TPSS										
$\mathbf{2}_{HIE}$	0.08	0.06	0.07	0.44	0.59	0.69	2.9	2.0	0.0	0.0	0.0
Wat419‡	0.00	0.00	0.00	0.12	0.93	0.88	5.6	6.5	57.0	−20.2	64.2
Wat492†	0.00	0.00	0.00	0.06	0.92	0.99	5.3	6.1	5.6	−16.0	66.6
W1†	0.00	0.00	0.00	0.05	0.95	0.97	6.1	6.4	81.2	−15.5	95.4
W2‡	0.00	0.00	0.00	0.19	0.79	0.88	6.8	6.0	69.7	−1.3	53.3
W3‡	0.00	0.00	0.00	0.97	1.01	0.00	4.2	5.1	65.5	−14.9	92.7
W4‡	0.05	0.00	0.00	0.17	0.81	0.93	8.6	8.1	76.6	−26.4	167.8
W5‡	0.05	0.00	0.00	0.18	0.86	0.86	8.7	9.1	69.0	−28.7	162.7
W6‡	0.00	0.00	0.00	0.12	0.83	0.96	4.4	3.6	62.7	−1.3	54.2
	B3LYP										
$\mathbf{2}_{HIE}$	0.08	0.07	0.08	0.51	0.57	0.67	2.9	2.0	0.0	0.0	0.0
Wat419†	0.00	0.00	0.00	0.00	1.02	0.95	5.6	6.5	61.4	−20.2	56.5
Wat492†	0.00	0.00	0.00	0.00	0.96	1.03	5.3	6.1	−1.9	−16.0	70.8
W1†	0.00	0.00	0.00	0.00	0.99	1.01	6.1	6.4	71.6	−15.5	99.0
W2‡	0.00	0.00	0.00	0.12	0.84	0.95	6.8	6.0	80.1	−1.3	73.7
W3†	0.00	0.00	0.00	0.00	0.97	1.02	4.2	5.1	54.7	−14.9	94.3
W4†	0.00	0.00	0.00	0.09	0.87	1.00	8.6	8.1	88.4	−26.4	198.7
W5‡	0.10	0.00	0.00	0.10	0.92	0.92	8.7	9.1	89.8	−28.7	182.0
W6†	0.00	0.00	0.00	0.05	0.88	1.02	4.4	3.6	60.2	−1.3	53.0

‡ QM/MM energy included in average dissociation energy of Cu(II) and $O_2^{\cdot -}$: 67 ± 7 kJ/mol ($n = 6$) with TPSS and 85 ± 7 kJ/mol ($n = 2$) with B3LYP. We generally assign the cases with a Cu spin density of 0.1 or higher as Cu(II) and $O_2^{\cdot -}$.
† QM/MM energy included in average dissociation energy of Cu(I) and O_2: 43 ± 54 kJ/mol ($n = 2$) with TPSS and 56 ± 31 kJ/mol ($n = 6$) with B3LYP.

Table S4 Mulliken spin populations and QM/MM energies for the reaction $2_{HIE} \longrightarrow 2^{dis}$ in triplet spin state, calculated with def2-TZVPP and surrounding point charges. Only atoms for which at least one spin population is greater than 0.05 are listed. Energies are relative to 2_{HIE} in the triplet state.

Residue	His37		His144	Cu	O_2		Distance (Å)		ΔE (kJ/mol)		
Atom	N	$N^{\delta 1}$	$N^{\varepsilon 2}$	Cu	O^1	O^2	$Cu-O^1$	$Cu-O^2$	QM/MM	MM	ptch
	TPSS										
$\mathbf{2}_{HIE}$	0.08	0.06	0.07	0.44	0.59	0.69	2.9	2.0	0.0	0.0	0.0
TS	0.13	0.07	0.07	0.50	0.43	0.69	3.8	2.6	100.9	-31.6	78.4
$\mathbf{2}^{dis}$	0.16	0.07	0.07	0.51	0.51	0.56	5.0	3.7	77.6	-22.6	23.9
	B3LYP										
$\mathbf{2}_{HIE}$	0.08	0.07	0.08	0.51	0.57	0.67	2.9	2.0	0.0	0.0	0.0
TS	0.14	0.08	0.08	0.62	0.39	0.64	3.8	2.6	88.7	-31.6	65.0
$\mathbf{2}^{dis}$	0.16	0.08	0.08	0.62	0.48	0.52	5.0	3.7	63.5	-22.6	0.1

Table S5 Mulliken spin populations and QM/MM energies for the dissociation of superoxide from 2_{HIE} in open-shell singlet spin state, calculated with def2-TZVPP and surrounding point charges. Only atoms for which at least one spin population is greater than 0.05 are listed. Energies are relative to 2_{HIE} in the triplet state.

Residue	His37		His144	Cu	O_2		Distance (Å)		ΔE (kJ/mol)		
Atom	N	$N^{\delta 1}$	$N^{\varepsilon 2}$	Cu	O^1	O^2	$Cu-O^1$	$Cu-O^2$	QM/MM	MM	ptch
	TPSS										
Wat419‡	−0.05	0.00	0.00	−0.16	0.13	0.14	5.5	6.5	80.0	−22.2	68.0
Wat492‡	−0.03	0.00	0.00	−0.11	0.08	0.08	5.3	6.0	32.6	−16.3	66.0
W1‡	−0.03	0.00	0.00	−0.12	0.09	0.09	6.0	6.2	109.7	−16.3	102.3
W2‡	−0.07	−0.01	−0.01	−0.23	0.21	0.16	6.8	5.9	88.3	−1.6	50.3
W3*	−0.04	−0.03	−0.04	−0.30	0.15	0.27	2.1	3.0	56.3	−19.9	100.5
W4‡	−0.06	−0.01	−0.01	−0.20	0.14	0.17	8.6	8.2	96.3	−26.8	159.1
W5‡	−0.06	−0.01	−0.01	−0.22	0.18	0.18	8.6	9.0	89.2	−28.3	158.6
W6‡	−0.05	−0.01	−0.01	−0.19	0.16	0.14	4.3	3.6	86.5	−3.9	61.8
	B3LYP										
Wat419‡	−0.03	0.00	0.00	−0.10	0.08	0.10	5.5	6.5	104.3	−22.2	63.5
Wat492†	0.00	0.00	0.00	−0.01	0.02	0.00	5.3	6.0	44.4	−16.3	71.5
W1†	0.00	0.00	0.00	−0.03	0.03	0.03	6.0	6.2	124.2	−16.3	104.2
W2‡	−0.06	−0.02	−0.01	−0.20	0.19	0.11	6.8	5.9	115.7	−1.6	63.0
W3*	−0.05	−0.05	−0.04	−0.40	0.16	0.39	2.1	3.0	67.5	−19.9	104.4
W4‡	−0.05	−0.01	−0.01	−0.15	0.08	0.15	8.6	8.2	124.8	−26.8	191.0
W5‡	−0.05	−0.01	−0.01	−0.18	0.14	0.14	8.6	9.0	125.4	−28.3	170.6
W6‡	−0.04	−0.02	−0.02	−0.16	0.13	0.11	4.3	3.6	103.0	−3.9	56.3

* During geometry optimization, superoxide binds back to Cu. $\mathbf{3}^{dis,W3}$ was therefore not included in the calculation of the average QM/MM energy.
‡ QM/MM energy included in average dissociation energy of Cu(II) and $O_2^{\bullet -}$: 83 ± 24 kJ/mol ($n = 8$) with TPSS and 115 ± 11 kJ/mol ($n = 5$) with B3LYP. We generally assign the cases with a Cu spin density of 0.1 or higher as Cu(II) and $O_2^{\bullet -}$.
† QM/MM energy included in average dissociation energy of Cu(I) and O_2: Not seen with TPSS and 84 ± 57 kJ/mol ($n = 2$) with B3LYP.

Table S6 Mulliken spin populations and QM/MM energies for the reaction $2_{HIE} \longrightarrow 2^{dis}$ in open-shell singlet spin state, calculated with def2-TZVPP and surrounding point charges. Only atoms for which at least one spin population is greater than 0.05 are listed. Energies are relative to 2_{HIE} in the triplet state. Note that negative HOMO-LUMO gaps were obtained for 2^{dis} in the geometry optimization with TPSS/def2-SV(P) and the single-point calculation with TPSS/def2-TZVPP and surrounding point charges.

Residue	His37		His144	Cu	O_2		Distance (Å)		ΔE (kJ/mol)		
Atom	N	$N^{\delta 1}$	$N^{\varepsilon 2}$	Cu	O^1	O^2	$Cu-O^1$	$Cu-O^2$	QM/MM	MM	ptch
	TPSS										
$\mathbf{2}_{HIE}$	0.09	0.06	0.08	0.43	-0.40	-0.26	2.0	2.9	9.4	-1.4	0.3
TS	-0.15	-0.08	-0.08	-0.51	0.35	0.53	3.8	2.6	104.1	-33.6	81.7
$\mathbf{2}^{dis}$	-0.17	-0.08	-0.08	-0.53	0.46	0.51	4.9	3.6	79.1	-26.0	31.7
	B3LYP										
$\mathbf{2}_{HIE}$	-0.09	-0.06	-0.08	-0.54	0.47	0.31	2.0	2.9	10.4	-1.4	-0.3
TS	-0.14	-0.09	-0.08	-0.63	0.37	0.60	3.8	2.6	89.6	-33.6	66.8
$\mathbf{2}^{dis}$	-0.16	-0.08	-0.08	-0.62	0.47	0.52	4.9	3.6	64.8	-26.0	6.6

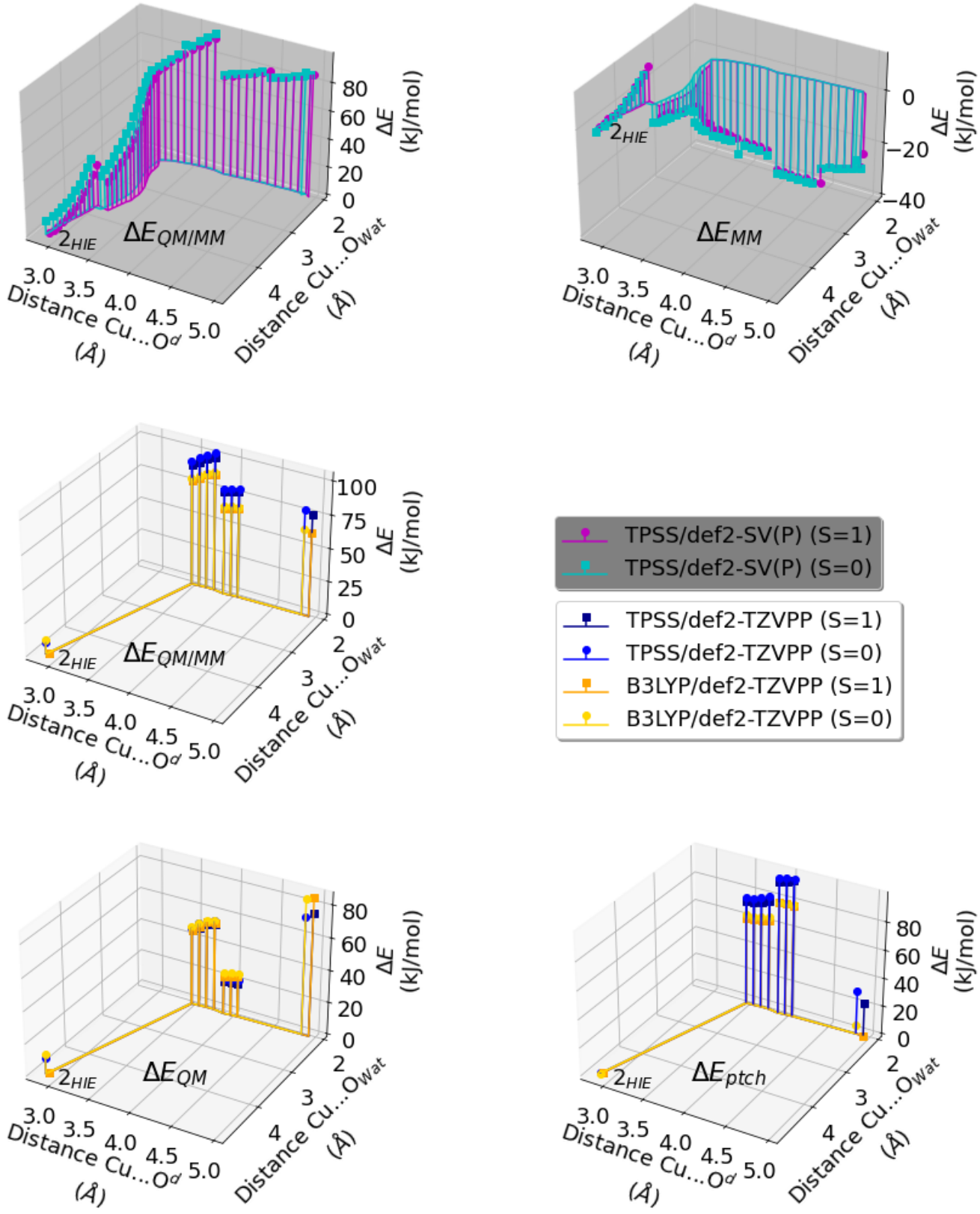

Fig. S6 Energies for the reaction $2_{HIE} \longrightarrow 2^{dis}$. The energy of 2_{HIE} in triplet state was used as reference. Top (gray background): $\Delta E_{QM/MM}$ energy and ΔE_{MM} obtained from geometry optimizations with TPSS/def2-SV(P) (for structures see Fig. S5). Middle and bottom (white background): $\Delta E_{QM/MM}$, ΔE_{QM} and ΔE_{ptch} obtained from single-point calculations with TPSS/def2-TZVPP and B3LYP/def2-TZVPP.

Table S7 Mulliken spin populations and QM/MM energies for the dissociation of $OOH^{\bullet}$ from 3_{int} in the triplet spin state, calculated with def2-TZVPP and surrounding point charges. Only atoms for which at least one spin population is greater than 0.06 are listed. Energies are relative to 3_{int} in the open-shell singlet state. If HOMO-LUMO gaps were negative in the calculations with point charges, ⊖ is added to the first column. If they were negative in the vacuum calculations (required to calculate the point charges contribution, ptch) ⊖ is added to the last column. In $OOH^{\bullet}$, the hydrogen is bonded to O^1.

Residue	His37		Asp140	His144	Cu	$OOH^{\bullet}$		H_2O	H_2O	Distance (Å)		ΔE (kJ/mol)		
Atom	N	$N^{\delta1}$	$O^{\delta1}$	$N^{\varepsilon2}$	Cu	O^1	O^2	O	O	$Cu-O^1$	$Cu-O^2$	QM/MM	MM	ptch
	TPSS													
Wat419*	0.16	0.09	0.00	0.09	0.53	0.43	0.57	0.05	0.00	7.3	6.9	5.0	5.5	34.2⊖
Wat492†	0.18	0.07	0.00	0.08	0.51	0.30	0.69	0.05	0.00	4.4	4.8	16.2	7.3	−46.3
W1†	0.17	0.08	0.00	0.08	0.52	0.28	0.72	0.05	0.00	6.4	6.7	71.2	−7.5	23.1
W2†	0.16	0.09	0.00	0.08	0.53	0.27	0.69	0.07	0.00	6.5	6.2	63.0	5.3	1.5
W3†	0.18	0.07	0.06	0.09	0.53	0.26	0.64	0.05	0.00	5.2	5.0	55.7	16.3	−71.2
W4†	0.17	0.08	0.00	0.08	0.52	0.30	0.70	0.06	0.00	8.0	7.8	13.9	−8.4	34.1
W5†	0.16	0.09	0.07	0.08	0.53	0.24	0.60	0.07	0.00	6.5	6.1	27.4	16.1	−53.2
W6†	0.15	0.08	0.00	0.09	0.54	0.26	0.64	0.08	0.08	4.3	3.5	51.5	20.6	−38.5
	B3LYP													
Wat419*	0.15	0.09	0.00	0.08	0.61	0.43	0.58	0.05	0.00	7.3	6.9	−56.2	5.5	37.4
Wat492†	0.17	0.08	0.00	0.08	0.60	0.29	0.72	0.05	0.00	4.4	4.8	−40.4	7.3	−60.5
W1†	0.16	0.08	0.00	0.08	0.61	0.26	0.74	0.05	0.00	6.4	6.7	10.6	−7.5	9.6
W2†	0.14	0.09	0.00	0.08	0.62	0.27	0.72	0.06	0.00	6.5	6.2	4.3	5.3	−79.6
W3†	0.16	0.08	0.00	0.09	0.61	0.27	0.74	0.04	0.00	5.2	5.0	−3.8	16.3	−91.5
W4†	0.16	0.08	0.00	0.08	0.61	0.29	0.72	0.05	0.00	8.0	7.8	−41.7	−8.4	25.4
W5†	0.15	0.09	0.00	0.08	0.61	0.27	0.73	0.06	0.00	6.5	6.1	−17.6	16.1	−64.5
W6†	0.14	0.08	0.00	0.09	0.62	0.26	0.70	0.07	0.05	4.3	3.5	−9.4	20.6	−51.9

* During geometry optimization, ASP90 is spontaneously protonated and O_2 forms. $\mathbf{3}^{dis,W419}$ was therefore not included in the calculation of the average QM/MM energy.
† QM/MM energy included in average dissociation energy: 43 ± 23 kJ/mol ($n = 7$) with TPSS and -14 ± 21 kJ/mol ($n = 7$) with B3LYP.

Table S8 Mulliken spin populations and QM/MM energies for the dissociation of $OOH^{\bullet}$ from 3_{int} in the open-shell singlet spin state, calculated with def2-TZVPP and surrounding point charges. Only atoms for which at least one spin population is greater than 0.06 are listed. Energies are relative to 3_{int} in the open-shell singlet state. If HOMO-LUMO gaps were negative in the calculations with point charges, ⊖ is added to the first column. If they were negative in the vacuum calculations (required to calculate the point charges contribution, ptch) ⊖ is added to the last column. In $OOH^{\bullet}$, the hydrogen is bonded to O^1.

Residue	His37		Asp140	His144	Cu	$OOH^{\bullet}$		H_2O	H_2O	Distance (Å)		ΔE (kJ/mol)		
Atom	N	$N^{\delta1}$	$O^{\delta1}$	$N^{\varepsilon2}$	Cu	O^1	O^2	O	O	$Cu-O^1$	$Cu-O^2$	QM/MM	MM	ptch
	TPSS													
$\mathbf{3}_{int}$	0.00	0.01	−0.08	0.01	0.06	0.02	0.06	0.00	0.00	1.9	2.8	0.0	0.0	0.0
Wat419*	−0.16	−0.09	0.00	−0.09	−0.53	0.43	0.57	−0.05	0.00	7.3	6.9	4.8	5.5	31.2⊖
Wat492†	−0.17	−0.07	−0.04	−0.08	−0.50	0.30	0.69	−0.05	0.00	4.4	4.8	15.8	6.9	−46.4⊖
W1†	−0.16	−0.08	−0.04	−0.07	−0.51	0.28	0.72	−0.05	0.00	6.4	6.7	71.0	−7.6	22.2⊖
W2†	0.16	0.09	0.00	0.09	0.53	−0.32	−0.66	0.07	0.00	6.2	5.9	19.3	6.3	−15.6
W3†	0.18	0.07	−0.07	0.09	0.54	−0.25	−0.63	0.05	0.00	5.2	5.0	54.9	16.2	−71.3
W4†	−0.16	−0.08	−0.03	−0.08	−0.51	0.30	0.70	−0.06	0.00	8.0	7.8	13.9	−8.3	31.6⊖
W5†	0.16	0.09	−0.08	0.08	0.53	−0.24	−0.59	0.07	0.00	6.5	6.1	27.0	15.9	−52.8
W6†	−0.15	−0.08	−0.02	−0.08	−0.53	0.26	0.65	−0.06	0.09	4.3	3.5	52.0	21.2	−41.9
	B3LYP													
$\mathbf{3}_{int}$	0.13	0.05	0.00	0.04	0.39	−0.21	−0.38	0.00	0.00	1.9	2.8	0.0	0.0	0.0
Wat419*	0.15	0.09	0.00	0.08	0.61	-0.43	−0.58	0.05	0.00	7.3	6.9	−56.5	5.5	36.8
Wat492†	−0.17	−0.08	0.00	−0.08	−0.60	0.28	0.71	−0.05	0.00	4.4	4.8	−40.4	6.9	−60.2
W1†	−0.16	−0.08	0.00	−0.08	−0.61	0.26	0.74	−0.05	0.00	6.4	6.7	10.6	−7.6	9.5
W2†	0.14	0.08	0.00	0.09	0.61	−0.31	−0.68	0.06	0.00	6.2	5.9	−38.6	6.3	−16.3
W3†	0.16	0.08	0.00	0.09	0.61	−0.27	−0.74	0.04	0.00	5.2	5.0	−3.9	16.2	−91.1
W4†	−0.16	−0.08	0.00	−0.08	−0.61	0.29	0.72	−0.05	0.00	8.0	7.8	−41.7	−8.3	25.1
W5†	0.15	0.09	0.00	0.08	0.61	−0.27	−0.73	0.06	0.00	6.5	6.1	−17.8	15.9	−63.6
W6†	−0.14	−0.08	0.00	−0.08	−0.62	0.25	0.69	−0.05	0.05	4.3	3.5	−8.9	21.2	−51.9

* During geometry optimization, ASP90 is spontaneously protonated and O_2 forms. $\mathbf{3}^{dis,W419}$ was therefore not included in the calculation of the average QM/MM energy.
† QM/MM energy included in average dissociation energy: 36 ± 23 kJ/mol ($n = 7$) with TPSS and -20 ± 21 kJ/mol ($n = 7$) with B3LYP.

Table S9 QM/MM energies for the dissociation of $OOH^{\bullet}$ from $\mathbf{3}_{int}$ in the closed-shell singlet spin state, calculated with def2-TZVPP and surrounding point charges. Energies are relative to $\mathbf{3}_{int}$ in the open-shell singlet state. If HOMO-LUMO gaps were negative in the calculations with point charges, $\ominus$ is added to the first column. If they were negative in the vacuum calculations (required to calculate the point charges contribution, ptch) $\ominus$ is added to the last column. In $OOH^{\bullet}$, the hydrogen is bonded to O^1.

	Distance (Å)		ΔE (kJ/mol)		
	Cu−O^1	Cu−O^2	QM/MM	MM	ptch
	TPSS				
$\mathbf{3}_{int}$	1.9	2.8	0.0	0.0	0.0
Wat419[†]	7.2	6.9	79.8	4.3	19.3
Wat492[†]	4.3	4.7	66.2	12.4	−40.6
W1[†]	6.4	6.6	152.1	−10.0	39.2
W2[†]	6.4	6.0	92.1	−1.8	5.9
W3[†]	4.9	4.2	108.5	8.1	−39.1
W4[†]	8.0	7.9	94.3	−15.6	74.6
W5[†]	6.4	6.3	84.3	20.5	−59.2
W6[†]	4.4	4.2	60.8	4.2	4.5
	B3LYP				
$\mathbf{3}_{int}$	1.9	2.8	0.0	0.0	0.0
Wat419[†]	7.2	6.9	133.2	4.3	28.8
Wat492[†]	4.3	4.7	114.1	12.4	−51.1
W1[†]	6.4	6.6	205.1	−10.0	35.1
W2[†]	6.4	6.0	144.7	−1.8	0.6
W3[†]	4.9	4.2	152.3	8.1	−49.3
W4[†]	8.0	7.9	161.4	−15.6	79.6
W5[†]	6.4	6.3	141.5	20.5	−70.4
W6[†]	4.4	4.2	72.5	4.2	−8.3

[†] QM/MM energy included in average dissociation energy: 92 ± 29 kJ/mol ($n = 7$) with TPSS and 141 ± 38 kJ/mol ($n = 7$) with B3LYP.

Table S10 Mulliken spin populations and QM/MM energies for the dissociation of $OOH^{\bullet}/OOH^{-}$ from $\mathbf{3l}^{red}$, calculated with def2-TZVPP and surrounding point charges. Only atoms for which at least one spin population is greater than 0.06 are listed. Energies are relative to $\mathbf{3l}^{red}$. Note that negative HOMO-LUMO gaps were obtained in the TPSS/def2-SV(P) calculation of W5. In $OOH^{\bullet}/OOH^{-}$, the hydrogen is bonded to O^1.

Residue	His37		His144	Cu	$OOH^{\bullet}/OOH^{-}$		H_2O	Distance (Å)		ΔE (kJ/mol)		
Atom	N	$N^{\delta 1}$	$N^{\varepsilon 2}$	Cu	O^1	O^2	O	$Cu-O^1$	$Cu-O^2$	QM/MM	MM	ptch
	TPSS											
$\mathbf{3l}^{red}$	0.09	0.08	0.07	0.48	0.03	0.22	0.00	2.0	2.7	0.0	0.0	0.0
Wat419†	0.05	0.03	0.03	0.32	0.20	0.31	0.02	6.5	6.2	101.9	−5.6	−39.9
Wat492†	0.11	0.07	0.07	0.48	0.05	0.09	0.08	4.5	5.0	37.5	10.1	−79.9
W1*	0.11	0.09	0.09	0.53	0.00	0.00	0.15	7.1	6.1	−1.6	0.4	−51.2
W2†	0.11	0.06	0.06	0.47	0.04	0.16	0.06	6.5	7.3	66.2	−6.8	−27.8
W3†	0.05	0.01	0.02	0.24	0.18	0.49	0.00	4.8	4.9	83.7	8.8	−56.8
W4†	0.08	0.04	0.04	0.38	0.12	0.28	0.03	8.1	8.0	57.1	−13.1	20.0
W5†	0.09	0.05	0.05	0.43	0.09	0.19	0.05	6.4	6.4	44.5	19.4	−98.5
W6*	0.10	0.09	0.09	0.53	0.00	0.02	0.14	4.9	3.9	34.7	3.5	−7.6
	B3LYP											
$\mathbf{3l}^{red}$	0.08	0.09	0.07	0.55	0.01	0.19	0.00	2.0	2.7	0.0	0.0	0.0
Wat419†	0.05	0.03	0.03	0.33	0.19	0.32	0.02	6.5	6.2	143.4	−5.6	−35.3
Wat492‡,†	0.12	0.08	0.08	0.60	0.00	0.00	0.08	4.5	5.0	48.8	10.1	−107.0
W1*	0.10	0.09	0.08	0.60	0.00	0.00	0.12	7.1	6.1	-7.1	0.4	−56.5
W2‡,†	0.13	0.08	0.08	0.62	0.00	0.00	0.07	6.5	7.3	79.2	−6.8	−57.1
W3†	0.04	0.01	0.02	0.18	0.19	0.56	0.00	4.8	4.9	103.1	8.8	−58.1
W4†	0.09	0.05	0.05	0.44	0.09	0.22	0.04	8.1	8.0	101.2	−13.1	18.6
W5‡,†	0.13	0.08	0.08	0.62	0.00	0.00	0.07	6.4	6.4	73.7	19.4	−112.3
W6*	0.09	0.08	0.08	0.60	0.00	0.00	0.12	4.9	3.9	37.0	3.5	−7.1

* $OOH^{\bullet}/OOH^{-}$ spontaneously abstracts a hydrogen atom from water during geometry optimization, leading to the formation of OH^{-} (coordinating to Cu) and H_2O_2. $\mathbf{3}^{dis,W1}$ and $\mathbf{3}^{dis,W6}$ were therefore not included in the calculation of the average QM/MM energy.

‡ QM/MM energy included in average dissociation energy of Cu(II) and OOH^{-}: 67 ± 16 kJ/mol ($n = 3$) with B3LYP (not seen with TPSS). We generally assign the cases with a Cu spin density of 0.1 or higher as Cu(II) and OOH^{-}.

† QM/MM energy included in average dissociation energy of Cu(II) and OOH^{-}, including states with higher character of Cu(I) and $OOH^{\bullet}$: 65 ± 24 kJ/mol ($n = 6$) with TPSS and 92 ± 32 kJ/mol ($n = 6$) with B3LYP.

Table S11 Mulliken spin populations and QM/MM energies for the reaction $\mathbf{3l}^{red} \longrightarrow \mathbf{3}^{red,dis}$, calculated with def2-TZVPP and surrounding point charges. Only atoms for which at least one spin population is greater than 0.06 are listed. Energies are relative to $\mathbf{3l}^{red}$. In OOH^{-}, the hydrogen is bonded to O^1.

Residue	His37		His144	Cu	$OOH^{\bullet}/OOH^{-}$		W_6	Distance (Å)		ΔE (kJ/mol)		
Atom	N	$N^{\delta 1}$	$N^{\varepsilon 2}$	Cu	O^1	O^2	O	$Cu-O^1$	$Cu-O^2$	QM/MM	MM	ptch
	TPSS											
$\mathbf{3l}^{red}$	0.09	0.08	0.07	0.48	0.22	0.03	0.00	2.0	2.7	0.0	0.0	0.0
TS	0.08	0.05	0.05	0.41	0.27	0.10	0.00	2.2	3.3	76.9	-8.4	4.5
$\mathbf{3}^{red,dis*}$	0.10	0.08	0.07	0.54	0.00	0.00	0.16	3.1	4.2	28.0	3.4	-12.6
	B3LYP											
$\mathbf{3l}^{red}$	0.08	0.09	0.07	0.55	0.19	0.01	0.00	2.0	2.7	0.0	0.0	0.0
TS	0.08	0.06	0.06	0.49	0.24	0.06	0.00	2.2	3.3	88.4	-8.4	-7.7
$\mathbf{3}^{red,dis*}$	0.09	0.08	0.07	0.62	0.00	0.00	0.14	3.1	4.2	29.3	3.4	-10.6

* OOH^{-} spontaneously abstracts a hydrogen atom from water during geometry optimization, leading to the formation of OH^{-} (coordinating to Cu) and H_2O_2.

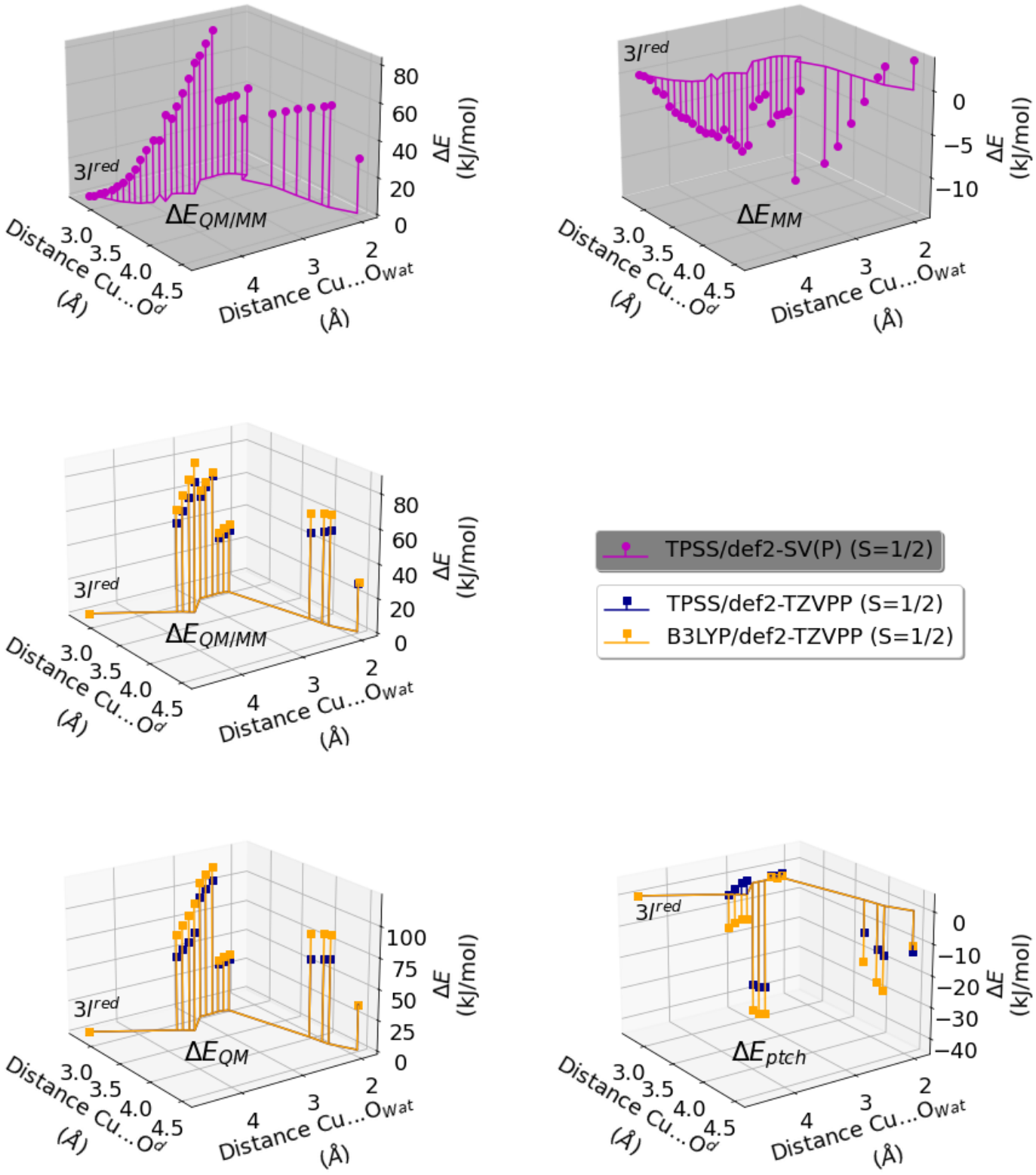

Fig. S7 Energies for the reaction $3I^{red} \longrightarrow 3^{red,dis}$. The energy of $3I^{red}$ was used as reference. Top (gray background): $\Delta E_{QM/MM}$ energy and ΔE_{MM} obtained from geometry optimizations with TPSS/def2-SV(P) (for structures see Fig. S5). Middle and bottom (white background): $\Delta E_{QM/MM}$, ΔE_{QM} and ΔE_{ptch} obtained from single-point calculations with TPSS/def2-TZVPP and B3LYP/def2-TZVPP.

Table S12 Mulliken spin populations and QM/MM energies for the dissociation of H_2O_2 from $4f^{red}$, calculated with def2-TZVPP and surrounding point charges. Only atoms for which at least one spin population is greater than 0.06 are listed (except if spin density is located on H_2O_2). Energies are relative to $4f^{red}$. In $OOH^{\bullet}/OOH^{-}$, the hydrogen is bonded to O^1.

Residue	His37		His144	Cu	H_2O_2		H_2O	Distance (Å)		ΔE (kJ/mol)		
Atom	N	$N^{\delta 1}$	$N^{\varepsilon 2}$	Cu	O^1	O^2	O	$Cu-O^1$	$Cu-O^2$	QM/MM	MM	ptch
	TPSS											
4f^{red}	0.17	0.07	0.08	0.50	0.05	0.02	0.00	2.1	3.2	0.0	0.0	0.0
Wat419†	0.17	0.07	0.08	0.51	0.00	0.00	0.05	7.1	7.9	5.9	4.0	14.6
Wat492†	0.17	0.08	0.08	0.51	0.00	0.00	0.06	4.3	3.4	6.0	−3.0	20.6
W1†	0.17	0.08	0.08	0.52	0.00	0.00	0.06	6.2	6.2	10.8	−1.0	50.0
W2†	0.17	0.07	0.09	0.52	0.00	0.00	0.06	6.7	6.6	8.5	2.5	11.9
W3†	0.17	0.07	0.08	0.51	0.00	0.00	0.05	5.0	5.8	14.4	17.5	−17.1
W4†	0.17	0.08	0.08	0.52	0.00	0.00	0.06	8.2	7.7	13.3	6.2	23.7
W5†	0.17	0.08	0.08	0.52	0.00	0.00	0.06	5.7	5.0	-10.4	14.2	−26.1
W6†	0.16	0.08	0.08	0.53	0.00	0.00	0.07	4.0	4.5	14.1	17.0	−23.7
	B3LYP											
4f^{red}	0.16	0.08	0.08	0.60	0.04	0.01	0.00	2.1	3.2	0.0	0.0	0.0
Wat419†	0.16	0.08	0.08	0.61	0.00	0.00	0.05	7.1	7.9	7.3	4.0	13.5
Wat492†	0.16	0.08	0.08	0.61	0.00	0.00	0.05	4.3	3.4	9.6	−3.0	30.4
W1†	0.16	0.08	0.08	0.61	0.00	0.00	0.05	6.2	6.2	8.6	−1.0	54.7
W2†	0.15	0.08	0.09	0.61	0.00	0.00	0.06	6.7	6.6	10.4	2.5	22.5
W3†	0.16	0.08	0.08	0.61	0.00	0.00	0.05	5.0	5.8	11.9	17.5	−16.4
W4†	0.15	0.08	0.08	0.61	0.00	0.00	0.05	8.2	7.7	14.3	6.2	30.4
W5†	0.16	0.08	0.08	0.61	0.00	0.00	0.05	5.7	5.0	-7.5	14.2	−23.3
W6†	0.14	0.08	0.08	0.61	0.00	0.00	0.06	4.0	4.5	12.5	17	−19.3

† QM/MM energy included in average dissociation energy of Cu(II) and H_2O_2: 8 ± 8 kJ/mol ($n = 8$) with TPSS and 8 ± 7 kJ/mol ($n = 8$) with B3LYP.

Table S13 Mulliken spin populations and QM/MM energies for the dissociation of H_2O_2 from $4f^{red}$, calculated with def2-TZVPP and surrounding point charges. Only atoms for which at least one spin population is greater than 0.06 are listed (except if spin density is located on H_2O_2). Energies are relative to $4f^{red}$. In $OOH^{\bullet}/OOH^{-}$, the hydrogen is bonded to O^1.

Residue	His37		His144	Cu	H_2O_2		W_6	Distance (Å)		ΔE (kJ/mol)		
Atom	N	$N^{\delta 1}$	$N^{\varepsilon 2}$	Cu	O^1	O^2	O	$Cu-O^1$	$Cu-O^2$	QM/MM	MM	ptch
	TPSS											
4f^{red}	0.17	0.07	0.08	0.50	0.05	0.02	0.00	2.1	3.2	0.0	0.0	0.0
TS	0.14	0.03	0.10	0.03	0.06	0.38	0.00	2.9	4.4	51.7	-9.3	39.0
4^{red,dis}	0.18	0.08	0.00	0.07	0.00	0.51	0.04	4.2	5.0	20.0	-26.3	72.1
	B3LYP											
4f^{red}	0.16	0.08	0.08	0.60	0.04	0.01	0.00	2.1	3.2	0.0	0.0	0.0
TS	0.21	0.05	0.05	0.54	0.00	0.00	0.00	2.9	4.4	66.9	-9.3	33.6
4^{red,dis}	0.17	0.09	0.07	0.61	0.00	0.00	0.00	4.2	5.0	21.3	-26.3	78.8

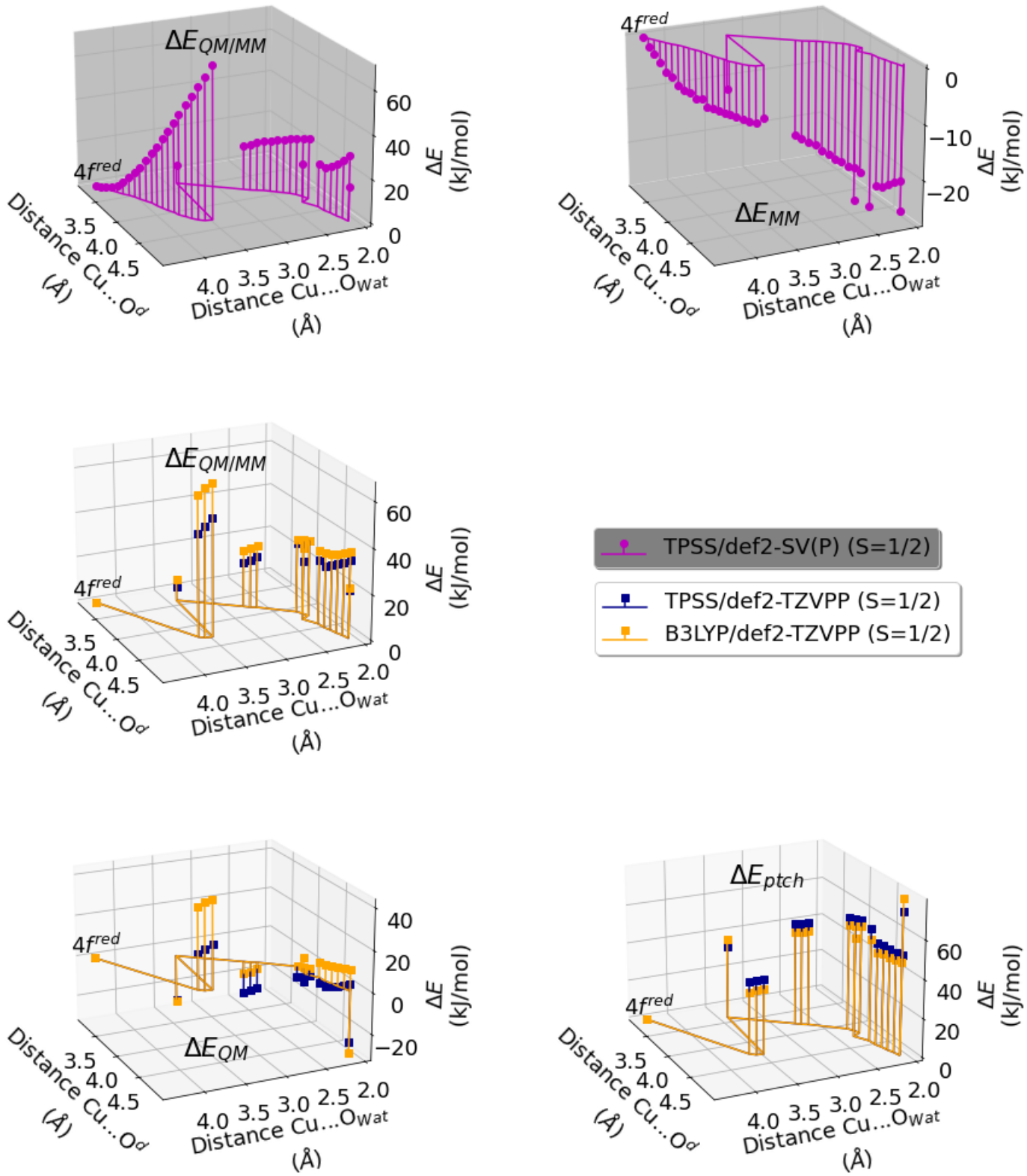

Fig. S8 Energies for the reaction $4f^{red} \longrightarrow 4^{red,dis}$. The energy of $4f^{red}$ was used as reference. Top (gray background): $\Delta E_{QM/MM}$ energy and ΔE_{MM} obtained from geometry optimizations with TPSS/def2-SV(P) (for structures see Fig. S5). Middle and bottom (white background): $\Delta E_{QM/MM}$, ΔE_{QM} and ΔE_{ptch} obtained from single-point calculations with TPSS/def2-TZVPP and B3LYP/def2-TZVPP.

First proton transfer

Formation of the $[Cu{-}OOH]^{2+}$ intermediate 3

Table S14 Intermediates and conformers obtained for the reaction $2_{HIP} \longrightarrow 3$. Negative HOMO-LUMO gaps are marked with ⊖. css stands for closed-shell singlet.

Conformers	Spin State	$\Delta E_{QM/MM}$ (kJ/mol) TPSS/def2-SV(P)	TPSS/def2-TZVPP	B3LYP/def2-TZVPP	Obtained by
2a$_{HIP}$	S=1	0.0	0.0	0.0	transferring proton back to HIS from **3b**
	S=0	10.5	9.6	10.0	
TS	S=1‡	36.0	23.2	60.0	TS of reaction **2a**$_{HIP} \longrightarrow$ **3a**
	S=0†	21.7	3.7	49.6	
3a	S=1	33.9	18.9	58.6	Product of reaction **2a**$_{HIP} \longrightarrow$ **3a**
	S=0	15.2	-5.8	48.7	
	S=0 (css)	18.0	-4.1	59.2	
2b$_{HIP}$	S=1	12.5	n/a	n/a	increasing QM region of **2**$_{HIP,small}$
	S=0	20.7	n/a	n/a	
3b	S=1	35.2	n/a	n/a	increasing QM region of **3**$_{small}$
	S=0	15.2	n/a	n/a	
2c$_{HIP}$	S=1	14.4	n/a	n/a	protonating **2**$_{HIE}$
	S=0	n/a	n/a	n/a	
TS$_{int}$	S=1	207.5⊖	178.0	235.0	TS of internal proton transfer
	S=0	194.1	158.6	229.6	
3$_{int}$	S=1	34.8 ⊖	19.4	56.4	Product of internal proton transfer*
	S=0	2.2	-22.6	26.1	
2d$_{HIP}$	S=1	21.8	2.5	−1.4	transferring proton back to HIS from **3**$_{int}$
	S=0	12.6	-8.1	11.8	
3d	S=1	35.8	17.2	48.2	Product of reaction **2d**$_{HIP} \longrightarrow$ **3d**
	S=0	2.2	-22.4	26.5	

‡ $O^{d}{-}H^{\varepsilon 2}$ distance is 1.10 Å.
† $O^{d}{-}H^{\varepsilon 2}$ distance is 1.14 Å.
* The OOH species turns during the transfer (see Fig. S9, S20 and S22), so that the hydrogen is again bound to the distal oxygen. This leads to a re-orientation of the hydrogen bond network, which could further stabilize intermediate **3**$_{int}$.

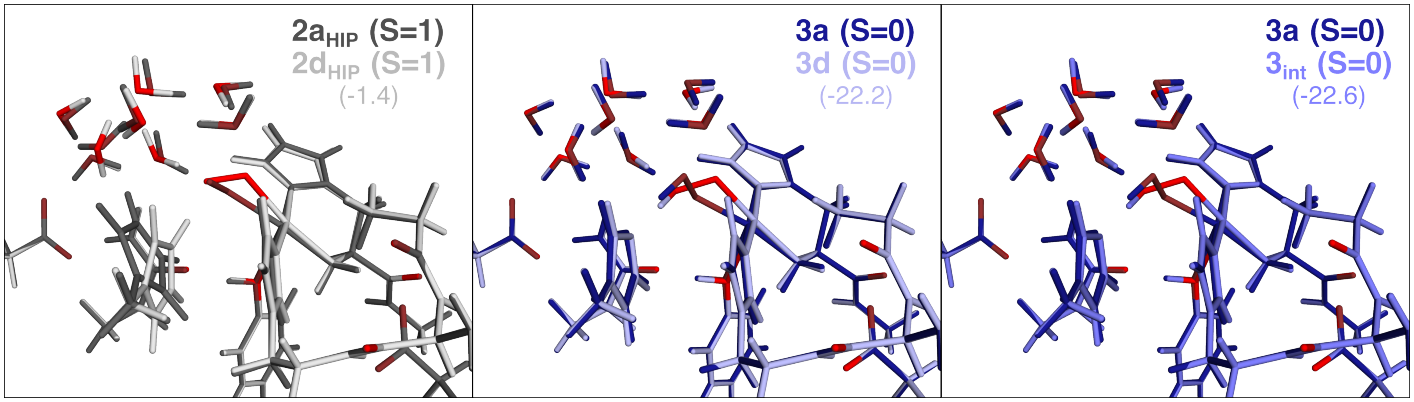

Fig. S9 Structures of selected conformers obtained for the reaction $2_{HIP} \longrightarrow 3$.

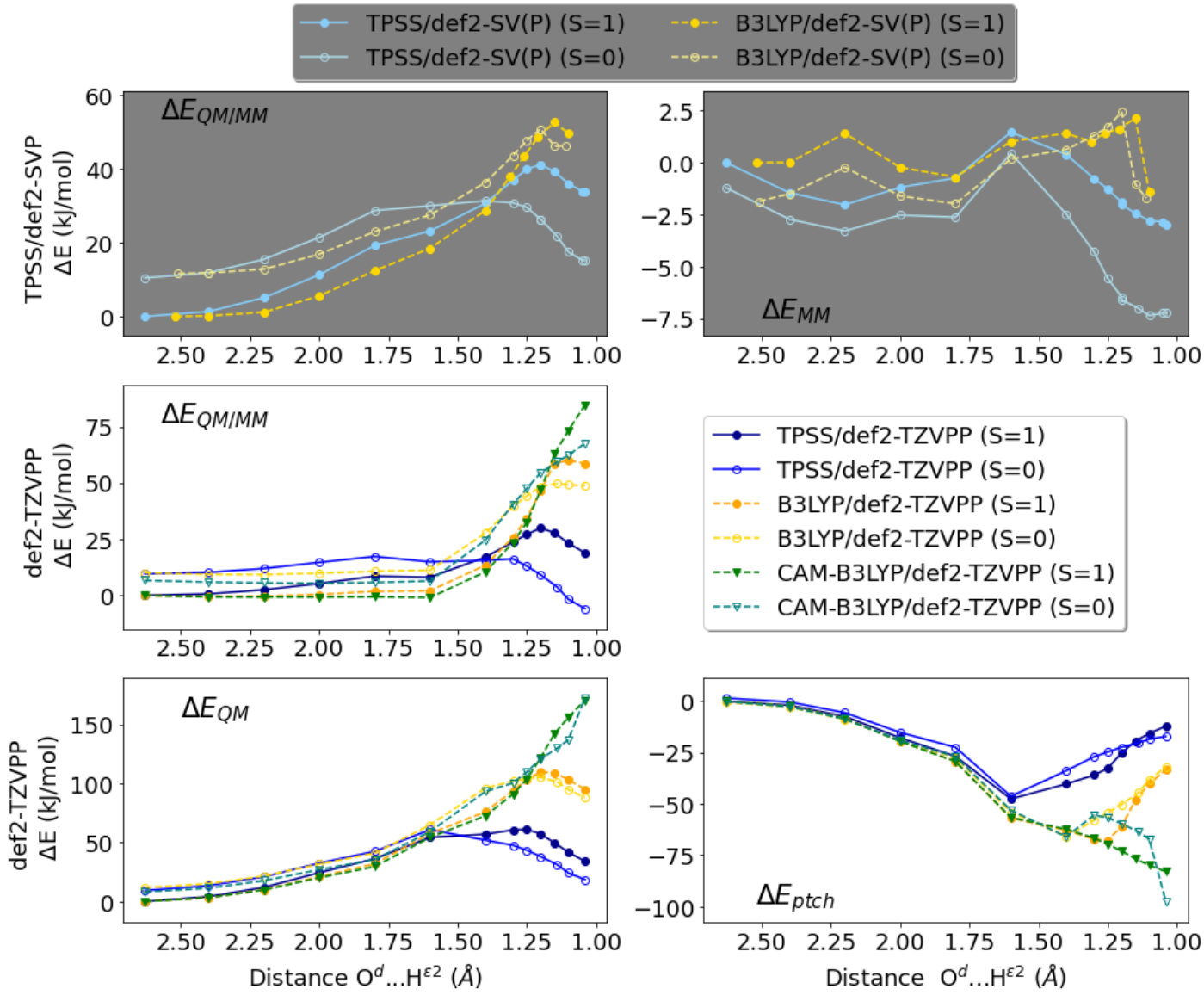

Fig. S10 Energies for the reaction $2a_{HIP} \longrightarrow 3a$. The energy of $2a_{HIP}$ in triplet state was used as reference. Top (gray background): $\Delta E_{QM/MM}$ energy and ΔE_{MM} obtained from geometry optimizations with TPSS/def2-SV(P) and B3LYP/def2-SV(P) (for structures see Fig. 2 and S11). Middle and bottom (white background): $\Delta E_{QM/MM}$, ΔE_{QM} and ΔE_{ptch} obtained from single-point calculations with TPSS/def2-TZVPP, B3LYP/def2-TZVPP and CAM-B3LYP/def2-TZVPP.

Table S15 $\langle S^2 \rangle$ for the open-shell singlet QM/MM and single-point calculations for the reaction $2a_{HIP} \longrightarrow 3a$.

Distance (Å)	TPSS/def2-SV(P)	TPSS/def2-TZVPP		B3LYP/def2-TZVPP		CAM-B3LYP/def2-TZVPP	
$O^d...H^{\varepsilon 2}$	QM/MM	ptch	QM	ptch	QM	ptch	QM
2.63 (**2a**$_{HIP}$)	1.00	1.00	1.00	1.01	1.01	1.01	1.01
2.40	1.00	n/a	n/a	n/a	n/a	n/a	n/a
2.20	1.00	n/a	n/a	n/a	n/a	n/a	n/a
2.00	1.00	n/a	n/a	n/a	n/a	n/a	n/a
1.80	1.00	n/a	n/a	n/a	n/a	n/a	n/a
1.60	0.95	0.96	0.90	1.00	1.00	1.00	1.00
1.40	0.63	0.54	0.65	0.90	0.87	0.97	0.91
1.30	0.39	0.06	0.46	0.74	0.74	0.85	0.85
1.25	0.28	0.07	0.50	0.70	0.74	0.83	0.84
1.20	0.20	0.08	0.54	0.65	0.75	0.81	0.82
1.14 (TS)	0.24	0.14	0.60	0.61	0.76	0.79	0.80
1.10	0.29	0.20	0.64	0.59	0.79	0.77	0.79
1.04 (**3a**)	0.33	0.24	0.69	0.58	0.82	0.73	1.01

Table S16 Mulliken spin populations for intermediates $2a_{HIP}$, 3a and 3_{int}, calculated with def2-TZVPP and surrounding point charges. Only atoms for which at least one spin population is greater than 0.06 are listed. In O_2/OOH, O^d and O^p are the oxygen atoms distal and proximal to Cu, respectively.

Residue	His37		Asp140		His144	Tyr213			Cu	O_2 / OOH	
Atom	N	$N^{\delta 1}$	$O^{\delta 1}$	$O^{\delta 2}$	$N^{\varepsilon 2}$	C^{γ}	C^{ζ}	O	Cu	O^d	O^p
	S=1										
2a$_{HIP}$, TPSS	0.08	0.06	0.00	0.00	0.06	0.00	0.00	0.00	0.42	0.70	0.63
2a$_{HIP}$, B3LYP	0.09	0.07	0.00	0.00	0.06	0.00	0.00	0.00	0.49	0.67	0.60
2a$_{HIP}$, CAM-B3LYP	0.09	0.07	0.00	0.00	0.06	0.00	0.00	0.00	0.55	0.64	0.57
3a, TPSS	0.11	0.08	0.13	0.09	0.07	0.08	0.04	0.05	0.50	0.20	0.41
3a, B3LYP	0.12	0.09	0.12	0.02	0.08	0.09	0.05	0.05	0.58	0.24	0.43
3a, CAM-B3LYP	0.15	0.09	0.00	0.00	0.08	0.00	0.00	0.00	0.64	0.35	0.64
3$_{int}$, TPSS	0.10	0.08	0.18	0.06	0.08	0.10	0.05	0.07	0.49	0.46	0.15
3$_{int}$, B3LYP	0.12	0.09	0.11	0.04	0.08	0.11	0.06	0.07	0.55	0.48	0.17
	S=0										
2a$_{HIP}$, TPSS	0.10	0.06	0.00	0.00	0.06	0.00	0.00	0.00	0.42	−0.43	−0.25
2a$_{HIP}$, B3LYP	−0.10	−0.07	0.00	0.00	−0.07	0.00	0.00	0.00	−0.53	0.51	0.26
2a$_{HIP}$, CAM-B3LYP	−0.10	−0.07	0.00	0.00	−0.07	0.00	0.00	0.00	−0.59	0.55	0.28
3a, TPSS	0.02	0.03	−0.11	−0.04	0.02	−0.03	−0.02	−0.02	0.13	0.02	0.07
3a, B3LYP	0.11	0.06	−0.03	−0.01	0.05	−0.04	−0.02	−0.03	0.47	−0.23	−0.26
3a, CAM-B3LYP	0.15	0.07	0.00	0.00	0.04	0.00	0.00	0.00	0.53	−0.33	−0.45
3$_{int}$, TPSS	0.00	0.01	−0.08	−0.03	0.01	0.00	0.00	0.00	0.06	0.06	0.02
3$_{int}$, B3LYP	0.13	0.05	0.00	0.00	0.04	0.00	0.00	0.00	0.39	−0.38	−0.21

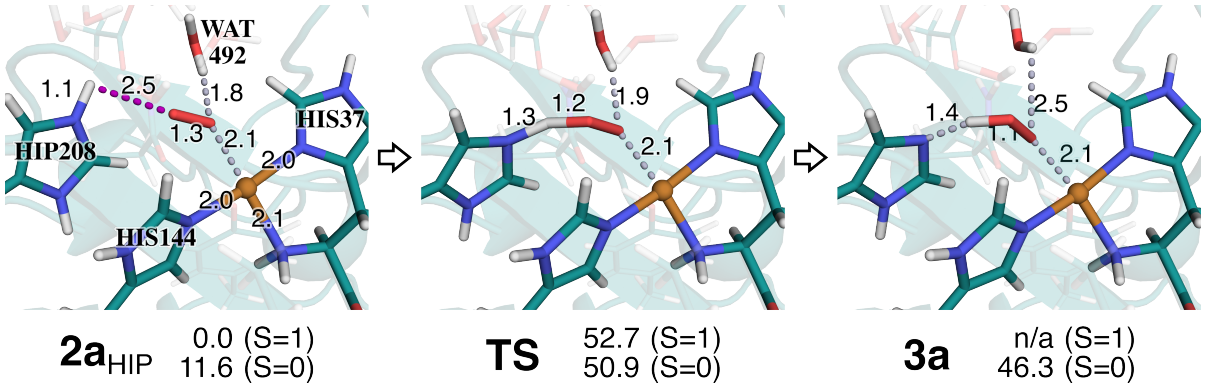

Fig. S11 Reaction 2a$_{HIP}$ ⟶ 3a. Structures were optimized with B3LYP/def2-SV(P), only the most stable electron configuration (triplet or open-shell singlet) is shown. Accordingly, we show here only the TS structure for the open-shell singlet with a $O^{d}...H^{\varepsilon 2}$ distance of 1.20 Å, but report the barrier for the triplet spin state at 1.15 Å (structure not shown). Energies were calculated with B3LYP/def2-SV(P) and are given in kJ/mol with reference to 2a$_{HIP}$. Distances are reported in Å and are omitted if they remain constant.

Formation of the [Cu−OOH]$^+$ intermediate 3^{red}

Table S17 Conformers obtained for the intermediate 3^{red}.

Conformers	Spin State	$\Delta E_{QM/MM}$ (kJ/mol) TPSS/def2-SV(P)	TPSS/def2-TZVPP	B3LYP/def2-TZVPP	Obtained by
3a^{red} ‡	S=1/2	0.0	0.0	0.0	reducing **2a**$_{HIP}$ (S=1)
3b^{red} ‡	S=1/2	−0.1	−0.6	−0.6	reducing **2a**$_{HIP}$ (S=0)
3c^{red} ‡	S=1/2	−15.0	n/a	n/a	reducing **2b**$_{HIP}$ (S=1)
3d^{red} †	S=1/2	65.0	n/a	n/a	reducing **2b**$_{HIP}$ (S=0)
3e^{red} ‡	S=1/2	0.0	n/a	n/a	reducing **2d**$_{HIP}$ (S=1)
3f^{red} ‡	S=1/2	−0.1	n/a	n/a	reducing **2d**$_{HIP}$ (S=0)
3g^{red} ‡	S=1/2	−43.8	n/a	n/a	protonating **2**$^{red}_{HIE}$
3h^{red} †	S=1/2	64.0	n/a	n/a	increasing QM region of **2a**$^{red}_{HIP,small}$
3i^{red}	S=1/2	−27.4	−26.5	−31.8	increasing QM region of **3b**$^{red}_{small}$
3j^{red}	S=1/2	−43.8	−28.9	−28.0	reducing **3a** (S=1)
3k^{red}	S=1/2	−43.8	−29.1	−28.2	reducing **3a** (S=0)
3l^{red}	S=1/2	−49.7	−28.4	−29.6	reducing **3**$_{int}$ (S=0)
TS$^{red}_{int}$	S=1/2	126.6	117.8	126.3	TS of internal proton transfer
3$^{red}_{int}$	S=1/2	−27.1	−29.3	−35.2	Product of internal proton transfer *

‡ Superoxide spontaneously abstracts a hydrogen atom from HIP during geometry optimization.
† Superoxide spontaneously abstracts a hydrogen atom from water during geometry optimization.
* The OOH species turns during the transfer (see Fig. S12, S21 and S23), so that the hydrogen is again bound to the distal oxygen. This leads to a re-orientation of the hydrogen bond network, which could further stabilize intermediate **3**$^{red}_{int}$.

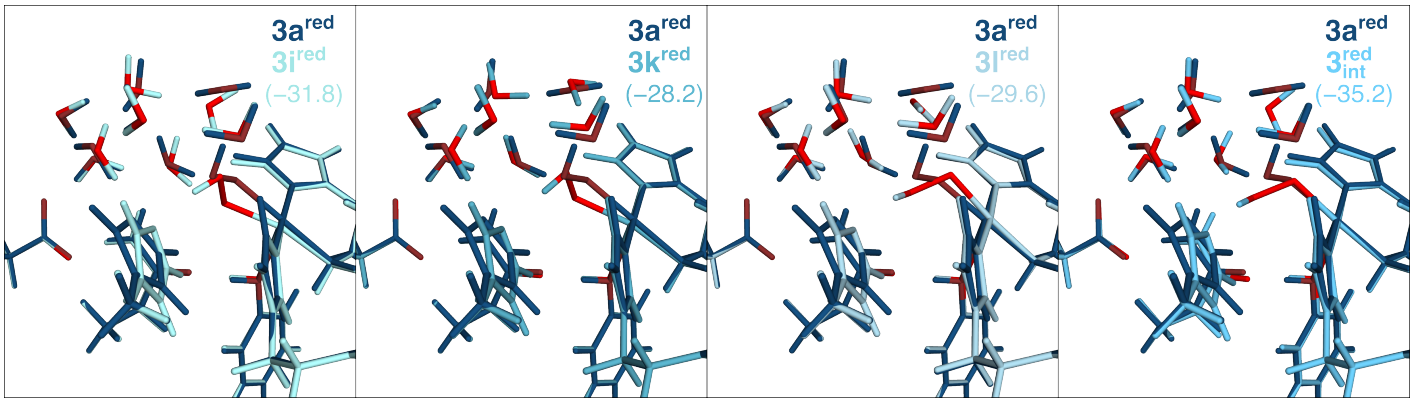

Fig. S12 Differences in structures of selected conformers of 3^{red}.

Table S18 Mulliken spin populations for intermediates $3a^{red}$, $3b^{red}$, $3j^{red}$, $3k^{red}$ and $3l^{red}$, calculated with def2-TZVPP and surrounding point charges. Only atoms for which at least one spin population is greater than 0.05 are listed. In OOH, O^d and O^p are the oxygen atoms distal and proximal to Cu, respectively.

Residue	His37		His144	Cu	OOH	
Atom	N	$N^{\delta 1}$	$N^{\varepsilon 2}$	Cu	O^d	O^p
3a^{red}, TPSS	0.07	0.07	0.07	0.44	0.08	0.23
3a^{red}, B3LYP	0.07	0.08	0.07	0.52	0.04	0.21
3b^{red}, TPSS	0.07	0.07	0.07	0.44	0.08	0.23
3b^{red}, B3LYP	0.07	0.08	0.07	0.52	0.04	0.21
3j^{red}, TPSS	0.07	0.07	0.06	0.46	0.06	0.23
3j^{red}, B3LYP	0.07	0.07	0.07	0.54	0.03	0.20
3k^{red}, TPSS	0.07	0.07	0.06	0.46	0.06	0.23
3k^{red}, B3LYP	0.07	0.07	0.07	0.54	0.03	0.20
3l^{red}, TPSS	0.09	0.08	0.07	0.48	0.03	0.22
3l^{red},B3LYP	0.08	0.09	0.07	0.55	0.01	0.19

To estimate the reaction energy for reaction $\mathbf{2}^{\mathrm{red}} \longrightarrow \mathbf{3}^{\mathrm{red}}$, we performed QM/MM calculations with a smaller QM region (see Fig. 1) and obtained intermediate $\mathbf{2a}^{\mathrm{red}}_{\mathrm{HIP,small}}$ by reducing $\mathbf{2}_{\mathrm{HIP,small}}$ in the triplet state (all other attempts to obtain $\mathbf{2}^{\mathrm{red}}_{\mathrm{HIP,small}}$ resulted in spontaneous formation of $\mathbf{3}^{\mathrm{red}}_{\mathrm{small}}$). The proton transfer $\mathbf{2a}^{\mathrm{red}}_{\mathrm{HIP,small}} \longrightarrow \mathbf{3a}^{\mathrm{red}}_{\mathrm{small}}$ (see Fig. S13 and S14) is downhill with a reaction energy of -119 kJ/mol (-100 kJ/mol with TPSS). Although we obtained large changes in MM energies with the small QM region, the MM energy for the proton transfer $\mathbf{2a}^{\mathrm{red}}_{\mathrm{HIP,small}} \longrightarrow \mathbf{3a}^{\mathrm{red}}_{\mathrm{small}}$ does not change more than 10 kJ/mol (see Fig. S14). Since the proton transfer is downhill with the small QM region and spontaneous with the larger one, we conclude that the proton transfer after reduction is highly favorable. Thus, if the second electron can be transferred, we consider reaction $\mathbf{2a}^{\mathrm{red}} \longrightarrow \mathbf{3a}^{\mathrm{red}}$ more likely than $\mathbf{2} \longrightarrow \mathbf{3}$. We also obtain a conformer $\mathbf{3b}^{\mathrm{red}}_{\mathrm{small}}$ that is -149 kJ/mol (-127 kJ/mol with TPSS) lower than $\mathbf{2a}^{\mathrm{red}}_{\mathrm{HIP,small}}$. However, the reduction potential from $\mathbf{2}_{\mathrm{HIP,small}}$ ($S = 1$) to $\mathbf{2}^{\mathrm{red}}_{\mathrm{HIP,small}}$ is -0.64 eV, showing that also this reduction is less likely than the reductions of later reaction intermediates.

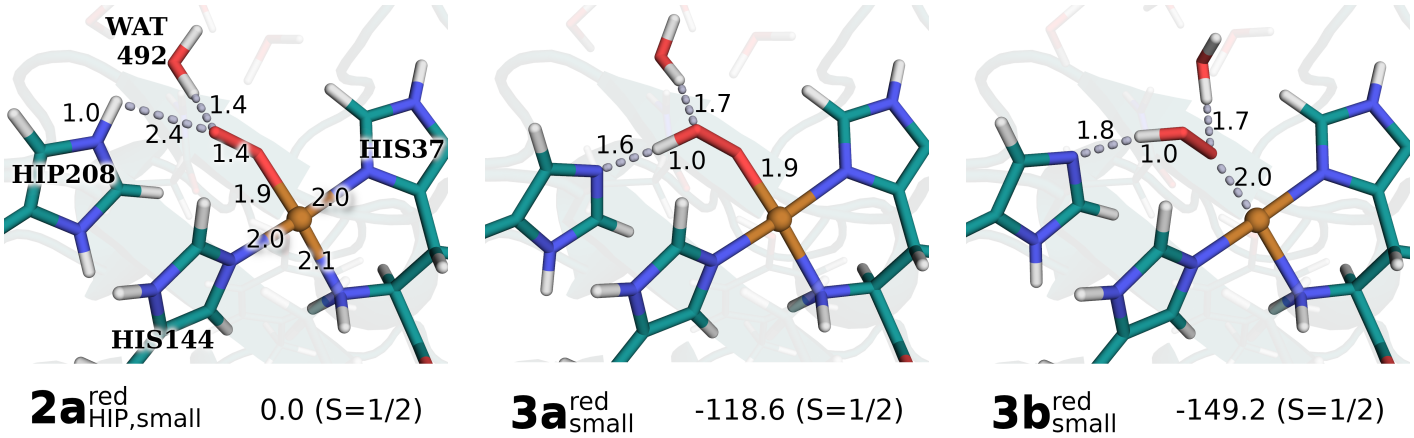

Fig. S13 Reaction $2a^{\mathrm{red}}_{\mathrm{HIP,small}} \longrightarrow 3a^{\mathrm{red}}_{\mathrm{small}}$ and conformer $3b^{\mathrm{red}}_{\mathrm{small}}$. Structures were optimized with TPSS/def2-SV(P). Distances are reported in Å. Omitted distances for $3a^{\mathrm{red}}_{\mathrm{small}}$ and $3b^{\mathrm{red}}_{\mathrm{small}}$ are identical to the distances reported for $2a^{\mathrm{red}}_{\mathrm{HIP,small}}$. Energies were calculated with B3LYP/def2-TZVPP and are given in kJ/mol with reference to $2a^{\mathrm{red}}_{\mathrm{HIP,small}}$.

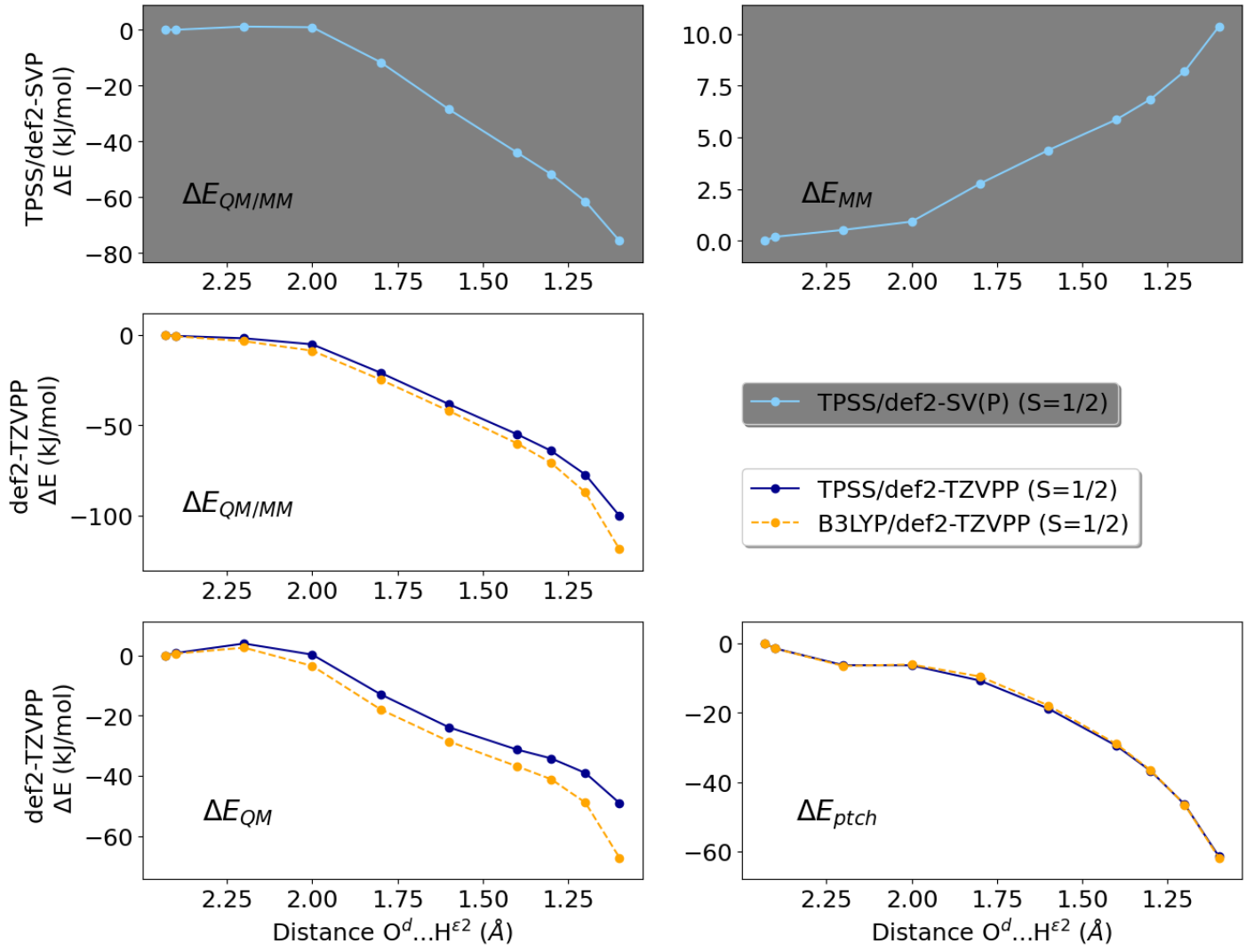

Fig. S14 Energies for the reaction $2a^{red}_{HIP,small} \longrightarrow 3a^{red}_{small}$ calculated with the small QM region. The energy of $2^{red}_{HIP,small}$ was used as reference. Top (gray background): $\Delta E_{QM/MM}$ energy and ΔE_{MM} obtained from geometry optimizations with TPSS/def2-SV(P) (for structures see Fig. S13). Middle and bottom (white background): $\Delta E_{QM/MM}$, ΔE_{QM} and ΔE_{ptch} obtained from single-point calculations with TPSS/def2-TZVPP and B3LYP/def2-TZVPP.

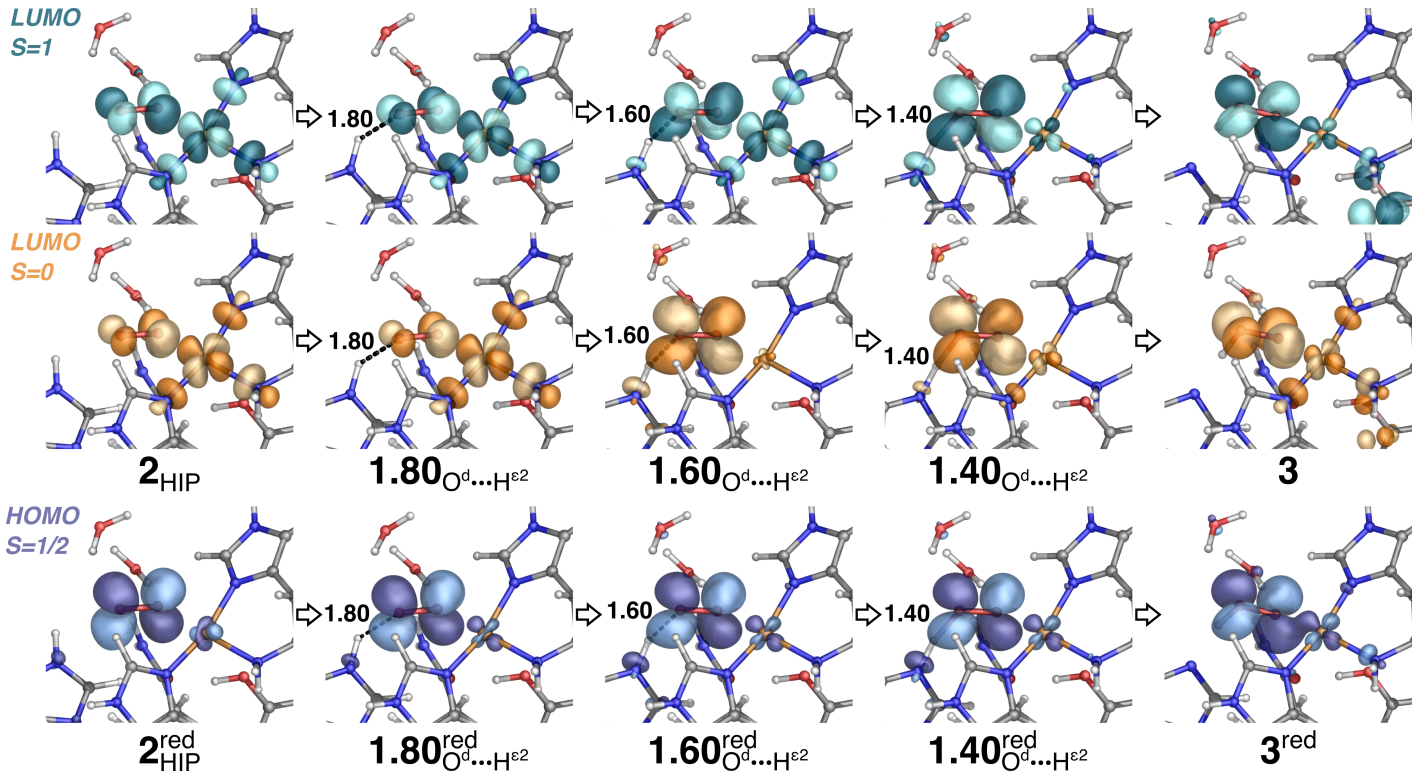

Fig. S15 Selected LUMOs for the reactant, product and selected $O^{d}...H^{\varepsilon 2}$ distances of 1.8, 1.6 and 1.4 Å for the reaction $2_{HIP} \longrightarrow 3$. HOMOs are shown for the same geometries but after reduction.

Second proton transfer

Formation of the $[Cu{-}H_2O_2]^{3+}$ intermediate 4

Table S19 Intermediates and conformers obtained for the reaction $3_{HIP} \longrightarrow 4$. Negative HOMO-LUMO gaps are marked with ⊖.

Intermediates/ Conformers	Spin State	$\Delta E_{QM/MM}$ (kJ/mol) TPSS/def2-SV(P)	TPSS/def2-TZVPP	B3LYP/def2-TZVPP	Obtained by
3a$_{HIP}$	S=1	9.6	13.7	2.1	protonating **3a**
	S=0	0.0	0.0	0.0	
TS1	S=1	33.5	36.1	17.7	TS1 of reaction **3a**$_{HIP} \longrightarrow$ **4a**
	S=0	25.0	25.7	16.5	
I	S=1	16.2	11.8	−6.6	I of reaction **3a**$_{HIP} \longrightarrow$ **4a**
	S=0	13.1	7.4	−9.9	
TS2	S=1	14.9	22.7	9.2	TS2 of reaction **3a**$_{HIP} \longrightarrow$ **4a**
	S=0	12.3	26.5	7.6	
4a	S=1	8.4	14.0	−3.7	Product of reaction **3a**$_{HIP} \longrightarrow$ **4a**
	S=0	6.1	11.7	−6.0	
3b$_{HIP}$ *	S=1	38.4	n/a	n/a	increasing QM region of **3**$_{HIP,small}$
	S=0	−6.9	n/a	n/a	
4b †	S=1	−26.1	−41.0	−65.6	increasing QM region of **4**$_{small}$
	S=0	−24.0	−40.4	−65.5	
3c$_{HIP}$	S=1	29.4 ⊖	n/a	n/a	protonating **3**$_{int}$
	S=0	15.2	n/a	n/a	

† An attempt to transfer the proton in **4b** back to HID208 failed, when releasing the restraint the proton always transferred back to form H_2O_2.

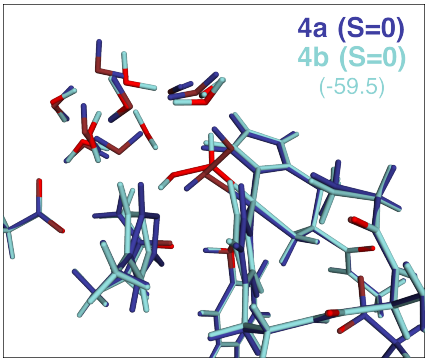

Fig. S16 Structures of selected conformers for the reaction $3_{HIP} \longrightarrow 4$.

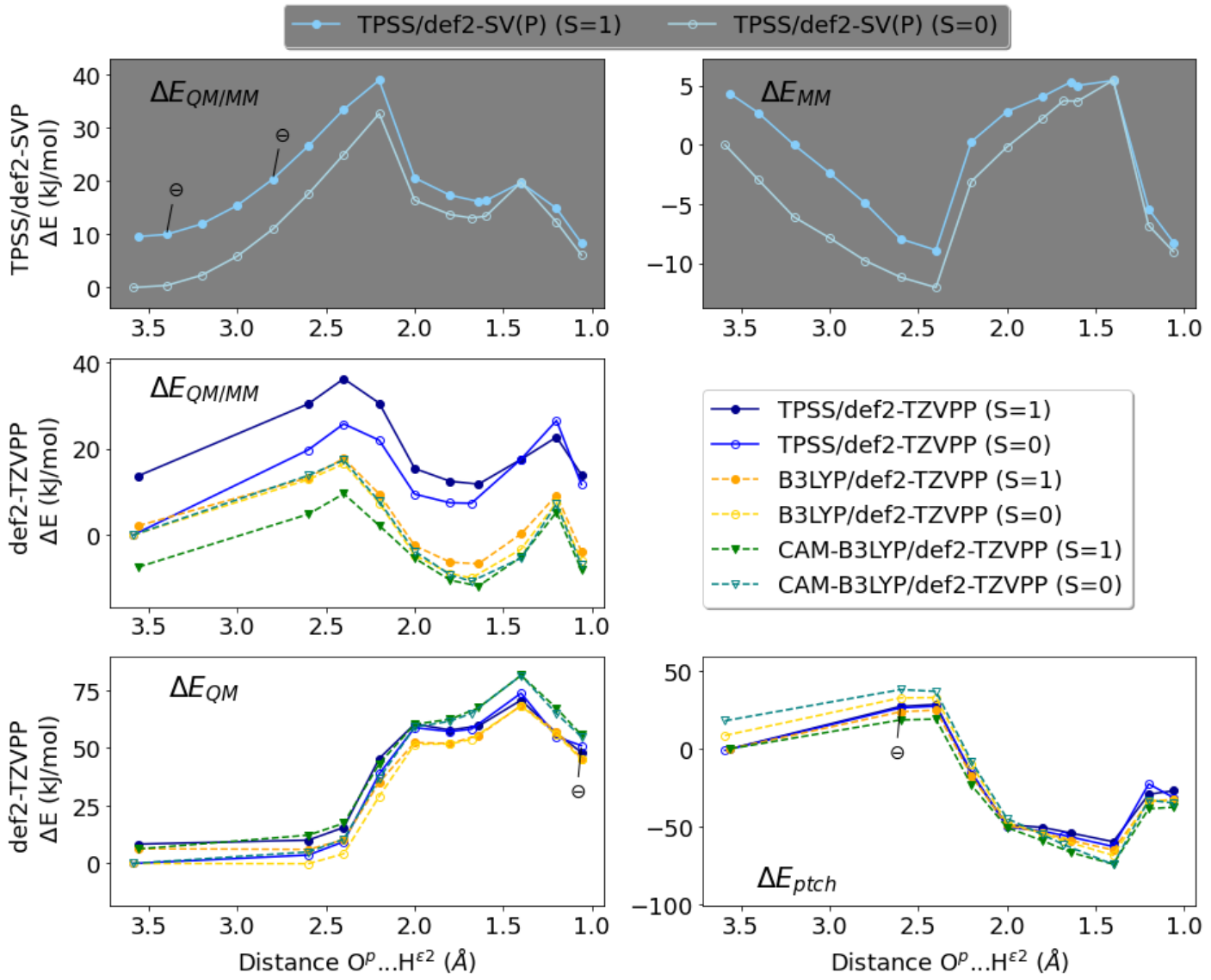

Fig. S17 Energies for the reaction $3a_{HIP} \longrightarrow 4a$. The energy of $3a_{HIP}$ in the open-shell singlet state was used as reference. Negative HOMO-LUMO gaps are marked with ⊖. $\Delta E_{QM/MM}$ energy and ΔE_{MM} obtained from geometry optimizations with TPSS/def2-SV(P) (for structures see Fig. 4). Middle and bottom (white background): $\Delta E_{QM/MM}$, ΔE_{QM} and ΔE_{ptch} obtained from single-point calculations with TPSS/def2-TZVPP, B3LYP/def2-TZVPP and CAM-B3LYP/def2-TZVPP.

Table S20 $\langle S^2 \rangle$ for the open-shell singlet QM/MM and single-point calculations for the reaction $3a_{HIP} \longrightarrow$ 4a calculated with the larger QM region.

Distance (Å) $O^p...H^{\varepsilon 2}$	TPSS/def2-SV(P) QM/MM	TPSS/def2-TZVPP ptch	TPSS/def2-TZVPP QM	B3LYP/def2-TZVPP ptch	B3LYP/def2-TZVPP QM
3.59 (**3a**$_{HIP}$)	0.68	0.62	0.94	0.89	1.01
3.40	0.68	n/a	n/a	n/a	n/a
3.20	0.69	n/a	n/a	n/a	n/a
3.00	0.71	n/a	n/a	n/a	n/a
2.80	0.72	n/a	n/a	n/a	n/a
2.60	0.74	0.70	0.98	0.95	1.01
2.40 (TS1)	0.76	0.72	0.98	0.96	1.01
2.20	0.79	0.75	1.00	0.97	1.01
2.00	0.83	0.78	1.00	0.98	1.01
1.80	0.90	0.85	1.00	1.00	1.01
1.68 (I)	0.94	0.89	1.00	1.00	1.01
1.60	0.96	n/a	n/a	n/a	n/a
1.40	1.00	0.99	1.00	1.01	1.01
1.20 (TS2)	1.00	1.00	1.00	1.01	1.01
1.06 (**4a**)	1.00	1.00	1.00	1.01	1.01

Table S21 Mulliken spin populations for intermediates $3a_{HIP}$, 4a and 4b, calculated with def2-TZVPP and surrounding point charges. Only atoms for which at least one spin population is greater than 0.07 are listed In OOH/H_2O_2, O^d and O^p are the oxygen atoms distal and proximal to Cu, respectively.

Residue	His37		Gly38	Asp140		Ser143	His144		Tyr213					Cu	OOH	/H_2O_2
Atom	N	$N^{\delta 1}$	N	$O^{\delta 1}$	$O^{\delta 2}$	O	N	$N^{\varepsilon 2}$	C^{γ}	C^{ζ}	O	$C^{\varepsilon 1}$	$C^{\varepsilon 2}$	Cu	O^d	O^p
	S=1															
3a$_{HIP}$, TPSS	0.10	0.09	0.05	0.20	0.12	0.05	0.05	0.07	0.13	0.06	0.08	0.00	0.04	0.51	0.07	0.25
3a$_{HIP}$, B3LYP	0.09	0.09	0.04	0.23	0.12	0.03	0.05	0.07	0.18	0.10	0.10	0.00	0.06	0.57	0.02	0.19
3a$_{HIP}$, CAM-B3LYP	0.09	0.08	0.00	0.00	0.00	0.00	0.00	0.07	0.38	0.11	0.22	0.21	0.14	0.60	0.00	0.16
4a, TPSS	0.16	0.08	0.04	0.21	0.13	0.08	0.09	0.08	0.15	0.08	0.09	0.00	0.05	0.54	0.00	0.09
4a, B3LYP	0.15	0.08	0.02	0.21	0.12	0.06	0.10	0.08	0.18	0.10	0.10	0.00	0.06	0.62	0.00	0.07
4a, CAM-B3LYP	0.14	0.08	0.00	0.00	0.00	0.00	0.00	0.09	0.38	0.10	0.22	0.21	0.14	0.65	0.00	0.06
4b, TPSS	0.15	0.09	0.03	0.20	0.12	0.08	0.08	0.08	0.15	0.08	0.09	0.00	0.05	0.52	0.07	0.03
4b, B3LYP	0.14	0.09	0.01	0.20	0.11	0.06	0.09	0.08	0.20	0.11	0.11	0.00	0.06	0.60	0.06	0.01
4b, CAM-B3LYP	0.13	0.09	0.00	0.00	0.00	0.00	0.00	0.08	0.38	0.11	0.23	0.21	0.13	0.64	0.00	0.05
	S=0															
3a$_{HIP}$, TPSS	0.06	0.06	−0.03	−0.18	−0.08	−0.03	−0.04	0.05	−0.09	−0.05	−0.05	0.00	−0.03	0.33	0.00	0.12
3a$_{HIP}$, B3LYP	0.07	0.08	−0.06	−0.22	−0.07	−0.02	−0.04	0.06	−0.14	−0.09	−0.08	0.00	−0.05	0.53	−0.02	0.11
3a$_{HIP}$, CAM-B3LYP	0.08	0.09	−0.02	−0.06	−0.02	0.00	0.00	0.07	−0.34	−0.08	−0.21	−0.19	−0.13	0.59	0.00	0.16
4a, TPSS	0.16	0.08	−0.05	−0.21	−0.12	−0.08	−0.09	0.09	−0.14	−0.08	−0.08	0.00	−0.05	0.53	0.00	0.09
4a, B3LYP	0.14	0.08	−0.05	−0.22	−0.10	−0.05	−0.09	0.08	−0.17	−0.10	−0.10	0.00	−0.06	0.62	0.00	0.07
4a, CAM-B3LYP	0.13	0.08	−0.01	−0.07	−0.02	0.00	0.00	0.09	−0.35	−0.09	−0.20	−0.19	−0.13	0.65	0.00	0.06
4b, TPSS	0.15	0.09	−0.04	−0.21	−0.11	−0.07	−0.06	0.08	−0.15	−0.08	−0.09	0.00	−0.05	0.51	0.07	0.03
4b, B3LYP	0.14	0.09	−0.03	−0.23	−0.10	−0.04	−0.07	0.08	−0.20	−0.11	−0.11	0.00	−0.06	0.60	0.06	0.01
4b, CAM-B3LYP	0.13	0.09	0.00	−0.01	0.00	0.00	0.00	0.08	−0.38	−0.10	−0.23	−0.20	−0.13	0.63	0.00	0.05

Formation of the $[Cu{-}H_2O_2]^{2+}$ intermediate 4^{red}

Table S22 Intermediates and conformers obtained for the reaction $3^{red}_{HIP} \longrightarrow 4^{red}$.

Conformers	Spin State	$\Delta E_{QM/MM}$ (kJ/mol)			Obtained by
		TPSS/def2-SV(P)	TPSS/def2-TZVPP	B3LYP/def2-TZVPP	
$\mathbf{3a}^{red}_{HIP}$	S=1/2	0.0	0.0	0.0	increasing QM region of $\mathbf{3}^{red}_{HIP,small}$
$\mathbf{TS1}^{red}$	S=1/2	10.8	15.2	15.0	TS1 of reaction $\mathbf{3a}^{red}_{HIP} \longrightarrow \mathbf{4a}^{red}$
$\mathbf{I}^{red}$	S=1/2	4.4	10.5	13.3	Intermediate of reaction $\mathbf{3a}^{red}_{HIP} \longrightarrow \mathbf{4a}^{red}$
$\mathbf{TS2}^{red}$	S=1/2	20.2	26.6	30.8	TS2 of reaction $\mathbf{3a}^{red}_{HIP} \longrightarrow \mathbf{4a}^{red}$
$\mathbf{4a}^{red}$	S=1/2	19.2	22.4	24.1	Product of reaction $\mathbf{3a}^{red}_{HIP} \longrightarrow \mathbf{4a}^{red}$
$\mathbf{4b}^{red}$	S=1/2	19.5	n/a	n/a	increasing QM region of $\mathbf{4}^{red}_{small}$
$\mathbf{3b}^{red}_{HIP}$	S=1/2	31.2	n/a	n/a	protonating $\mathbf{3l}^{red}$
$\mathbf{3c}^{red}_{HIP}$	S=1/2	25.4	n/a	n/a	protonating $\mathbf{3j}^{red}$
$\mathbf{3d}^{red}_{HIP}$	S=1/2	38.2	n/a	n/a	reducing $\mathbf{3a}_{HIP}$ (S=1)
$\mathbf{3e}^{red}_{HIP}$	S=1/2	37.3	n/a	n/a	reducing $\mathbf{3a}_{HIP}$ (S=0)
$\mathbf{4c}^{red}$	S=1/2	16.9	n/a	n/a	reducing **4a** (S=1)
$\mathbf{4d}^{red}$	S=1/2	16.8	n/a	n/a	reducing **4a** (S=0)
$\mathbf{4e}^{red}$	S=1/2	−20.5	−25.0	−29.2	reducing **4b** (S=1)
$\mathbf{4f}^{red}$ †	S=1/2	−20.6	−25.6	−30.0	reducing **4b** (S=0)

† An attempt to transfer the proton in $\mathbf{4f}^{red}$ back to HID208 failed, when releasing the restraint the proton always transferred back to form H_2O_2.

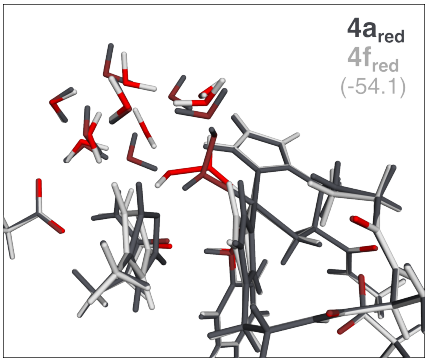

Fig. S18 Structures of selected conformers for the reaction $3^{red}_{HIP} \longrightarrow 4^{red}$.

Table S23 Mulliken spin populations for intermediates $3a^{red}_{HIP}$, $4a^{red}$ and $4f^{red}$, calculated with def2-TZVPP and surrounding point charges. Only atoms for which at least one spin population is greater than 0.05 are listed. In H_2O_2, O^d and O^p are the oxygen atoms distal and proximal to Cu, respectively.

Residue	His37		His144	Cu	H_2O_2
Atom	N	$N^{\delta 1}$	$N^{\varepsilon 2}$	Cu	O^p
$\mathbf{3a}^{red}_{HIP}$, TPSS	0.12	0.08	0.08	0.50	0.15
$\mathbf{3a}^{red}_{HIP}$, B3LYP	0.11	0.09	0.08	0.58	0.12
$\mathbf{3a}^{red}_{HIP}$, CAM-B3LYP	0.11	0.08	0.07	0.62	0.11
$\mathbf{4a}^{red}$, TPSS	0.18	0.06	0.08	0.51	0.06
$\mathbf{4a}^{red}$, B3LYP	0.17	0.07	0.08	0.60	0.05
$\mathbf{4a}^{red}$, CAM-B3LYP	0.16	0.07	0.08	0.64	0.04
$\mathbf{4f}^{red}$, TPSS	0.17	0.07	0.08	0.50	0.05
$\mathbf{4f}^{red}$, B3LYP	0.16	0.08	0.08	0.60	0.04
$\mathbf{4f}^{red}$, CAM-B3LYP	0.15	0.08	0.08	0.64	0.03

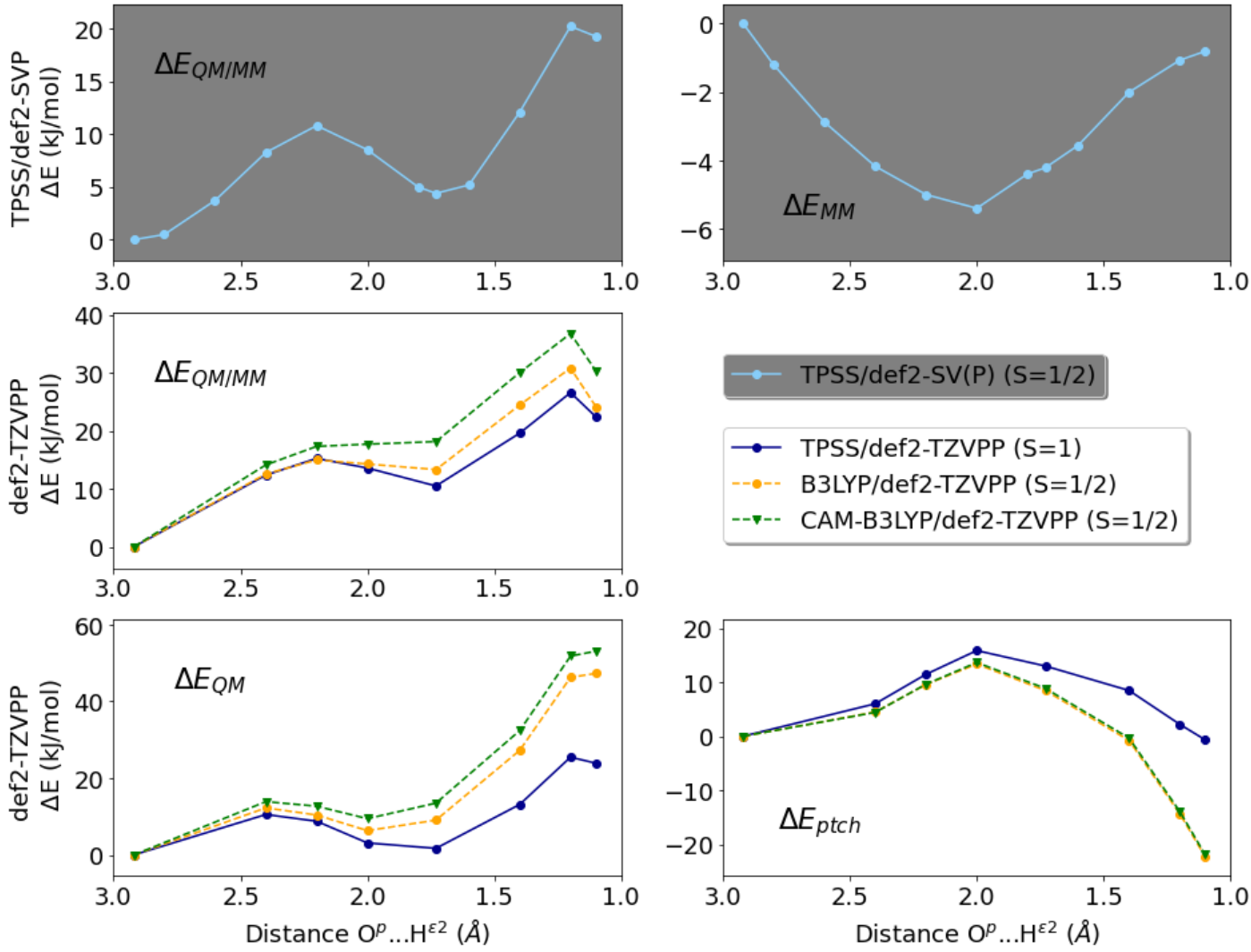

Fig. S19 Energies for the reaction $3a^{red}_{HIP} \longrightarrow 4a^{red}$. The energy of $3a^{red}_{HIP}$ was used as reference. Negative HOMO-LUMO gaps are marked with ⊖. Top (gray background): $\Delta E_{QM/MM}$ energy and ΔE_{MM} obtained from geometry optimizations with TPSS/def2-SV(P) (for structures see Fig. 5). Middle and bottom (white background): $\Delta E_{QM/MM}$, ΔE_{QM} and ΔE_{ptch} obtained from single-point calculations with TPSS/def2-TZVPP, B3LYP/def2-TZVPP and CAM-B3LYP/def2-TZVPP.

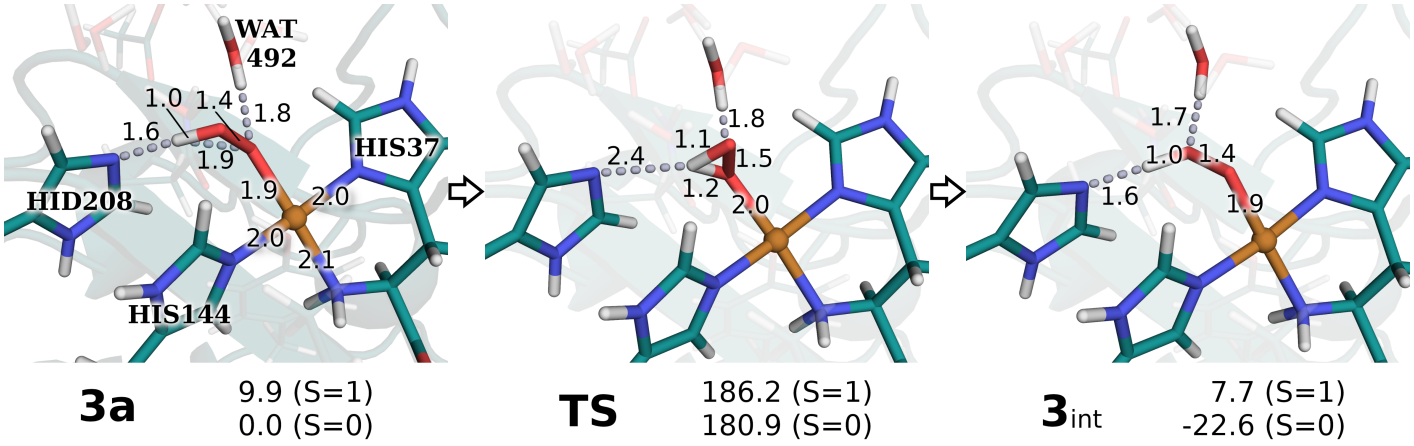

Fig. S20 Reaction 3a $\longrightarrow 3_{int}$. Structures were optimized with TPSS/def2-SV(P). Distances are reported in Å and are omitted if they remain constant. Energies were calculated with B3LYP/def2-TZVPP and are given in kJ/mol relatove to 3a in the open-shell singlet state.

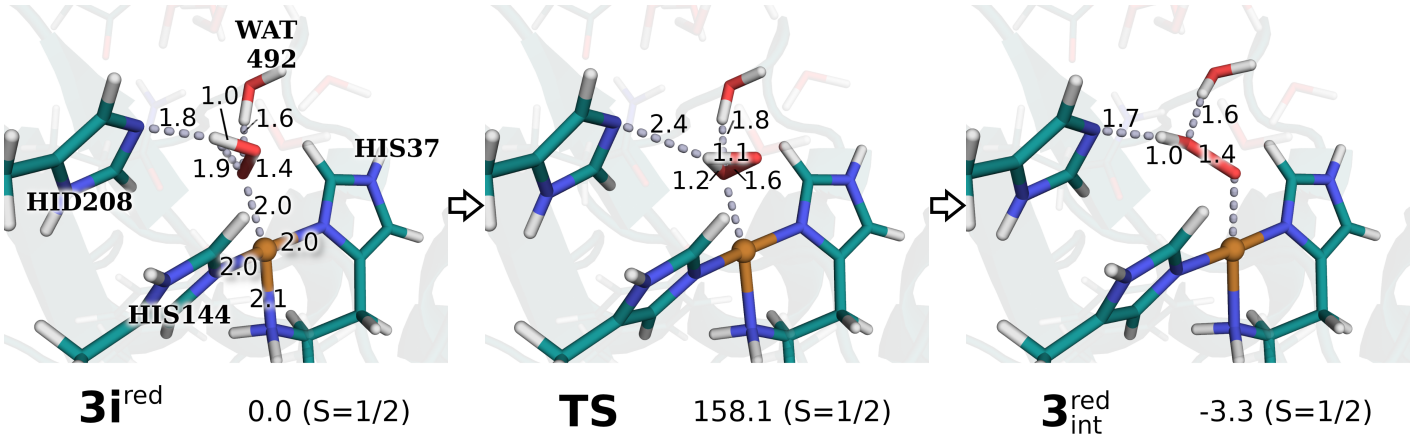

Fig. S21 Reaction $3i^{red} \longrightarrow 3^{red}_{int}$. Structures were optimized with TPSS/def2-SV(P). Distances are reported in Å and are omitted if they remain constant. Energies were calculated with B3LYP/def2-TZVPP and are given in kJ/mol relative to $3i^{red}$.

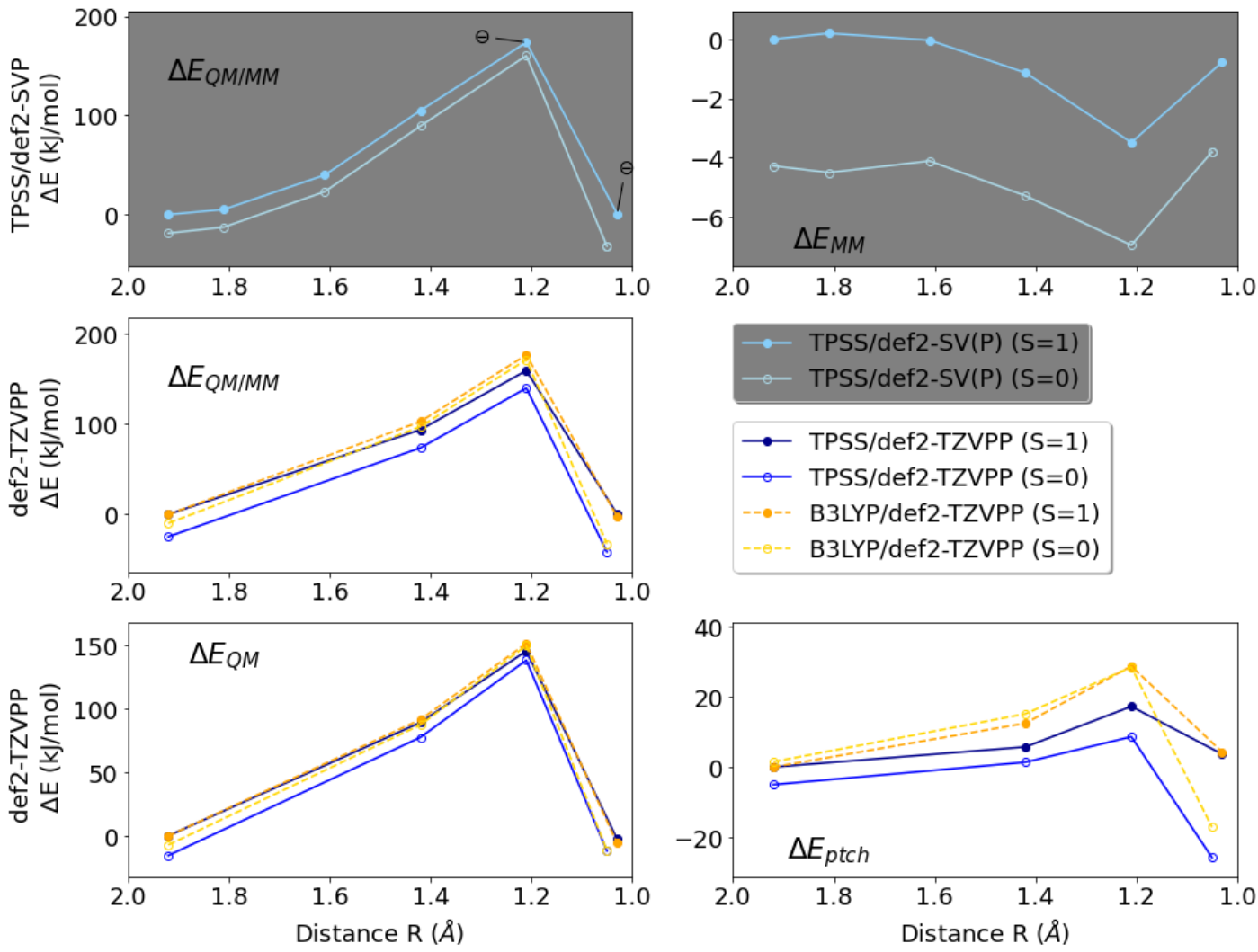

Fig. S22 Energies for the internal proton transfer 3a ⟶ 3_{int}. The energy of 3a in triplet state was used as reference. Distance R between O^2_{O2} and $H^{\varepsilon 2}$ in Å. Negative HOMO-LUMO gaps were obtained for energies marked with ⊖. Top (gray background): $\Delta E_{QM/MM}$ energy and ΔE_{MM} obtained from geometry optimizations with TPSS/def2-SV(P) (for structures see Fig. S20). Middle and bottom (white background): $\Delta E_{QM/MM}$, ΔE_{QM} and ΔE_{ptch} obtained from single-point calculations with TPSS/def2-TZVPP and B3LYP/def2-TZVPP.

Table S24 $\langle S^2 \rangle$ for the open-shell singlet QM/MM and single-point calculations for the reaction 3a ⟶ 3_{int}. Corresponding Mulliken spin populations are reported in Table S16.

Distance (Å) $O^2 \ldots H^{\varepsilon 2}$	TPSS/def2-SV(P) QM/MM	TPSS/def2-TZVPP ptch	TPSS/def2-TZVPP QM	B3LYP/def2-TZVPP ptch	B3LYP/def2-TZVPP QM
1.92 (**3a**)	0.33	0.24	0.69	0.58	0.82
1.81	0.35	n/a	n/a	n/a	n/a
1.61	0.36	n/a	n/a	n/a	n/a
1.42	0.42	0.33	0.77	0.67	0.92
1.21 (TS)	0.53	0.45	0.88	0.77	1.00
1.05 ($\mathbf{3}_{int}$)	0.24	0.12	0.44	0.46	0.72

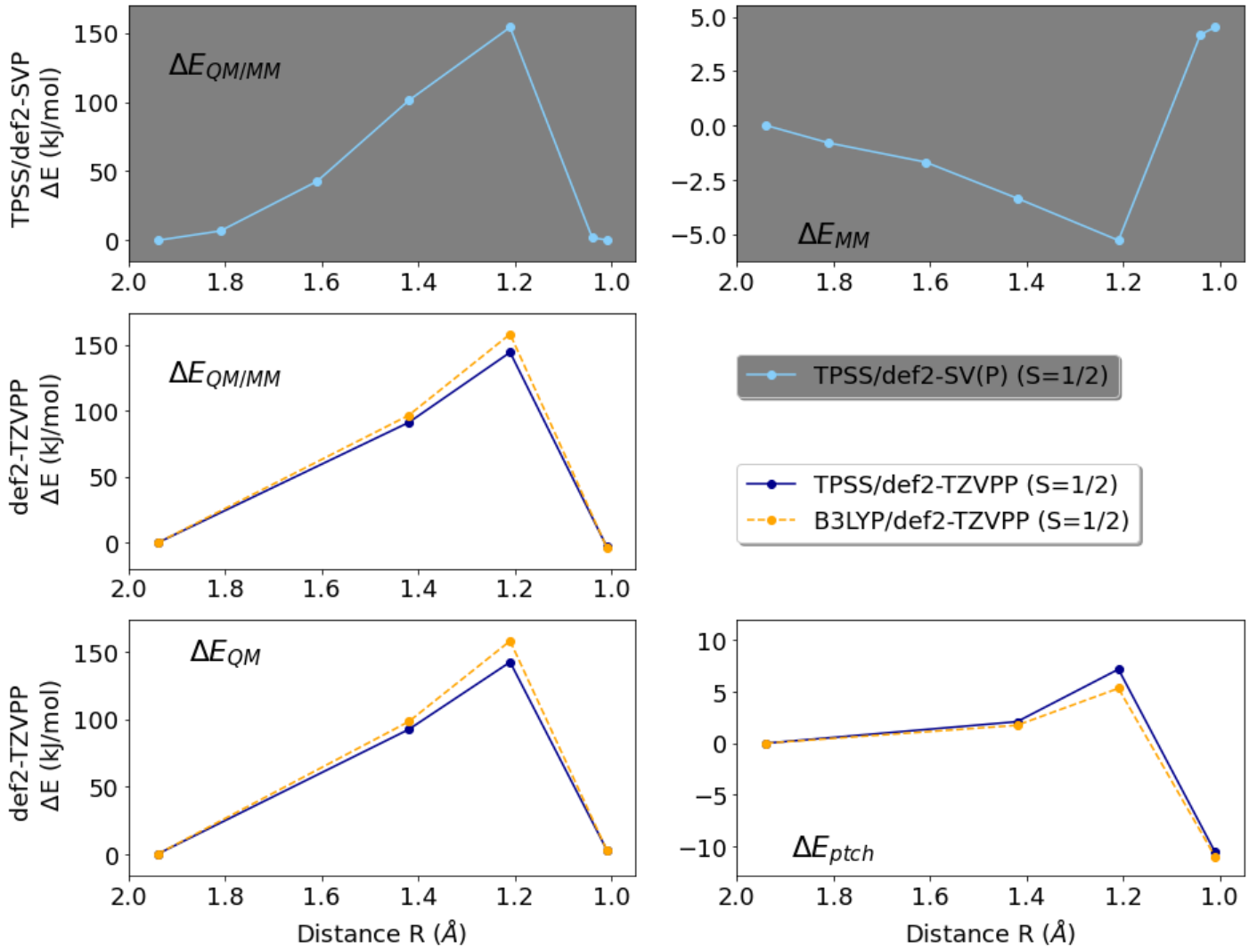

Fig. S23 Energies for the internal proton transfer $3i^{red} \longrightarrow 3^{red}_{int}$. The energy of $3i^{red}$ in triplet state was used as reference. Distance R between O^2_{O2} and $H^{\epsilon 2}$ in Å. Negative HOMO-LUMO gaps were obtained for energies marked with $\ominus$. Top (gray background): $\Delta E_{QM/MM}$ energy and ΔE_{MM} obtained from geometry optimizations with TPSS/def2-SV(P) (for structures see Fig. S21). Middle and bottom (white background): $\Delta E_{QM/MM}$, ΔE_{QM} and ΔE_{ptch} obtained from single-point calculations with TPSS/def2-TZVPP and B3LYP/def2-TZVPP.

Notes and references

1 N. Kruer-Zerhusen, M. Alahuhta, V. V. Lunin, M. E. Himmel, Y. J. Bomble and D. B. Wilson, Structure of a Thermobifida fusca lytic polysaccharide monooxygenase and mutagenesis of key residues, *Biotechnol Biofuels*, 2017, **10**, 243.

2 Z. Forsberg, A. MacKenzie, M. Sørlie, Å. K. Røhr, R. Helland, A. S. Arvai, G. Vaaje-Kolstad and V. G. H. Eijsink, Structural and functional characterization of a conserved pair of bacterial cellulose–oxidizing lytic polysaccharidemonooxygenases, *Proc. Sci. Nat. USA*, 2014, **111**, 8446–8451.

3 *Maestro version 2021-1*, Schrödinger, LLC, New York, NY, 2021.

4 M. H. M. Olsson, C. R. Søndergard, M. Rostkowski and J. H. Jensen, PROPKA3: Consistent Treatment of Internal and Surface Residues in Empirical pKa predictions, *J. Chem. Theory Comput.*, 2011, **7**, 525–537.

5 R. J. Quinlan, M. D. Sweeney, L. Lo Leggio, H. Otten, J.-C. N. Poulsen, K. S. Johansen, K. B. R. M. Krogh, C. I. Jørgensen, M. Tovborg, A. Anthonsen, T. Tryfona, C. P. Walter, P. Dupree, F. Xu, G. J. Davies and P. H. Walton, Insights into the oxidative degradation of cellulose by a copper metalloenzyme that exploits biomass components, *Proc. Natl. Acad. Sci.*, 2011, **108**, 15079–15084.

6 S. G. Balasubramani, G. P. Chen, S. Coriani, M. Diedenhofen, M. S. Frank, Y. J. Franzke, F. Furche, R. Grotjahn, M. E. Harding, C. Hättig, A. Hellweg, B. Helmich-Paris, C. Holzer, U. Huniar, M. Kaupp, A. Marefat Khah, S. Karbalaei Khani, T. Müller, F. Mack, B. D. Nguyen, S. M. Parker, E. Perlt, D. Rappoport, K. Reiter, S. Roy, M. Rückert, G. Schmitz, M. Sierka, E. Tapavicza, D. P. Tew, C. van Wüllen, V. K. Voora, F. Weigend, A. Wodyński and J. M. Yu, TURBOMOLE: Modular program suite for ab initio quantum-chemical and condensed-matter simulations, *J. Chem. Phys.*, 2020, **152**, 184107.

7 J. Tao, J. P. Perdew, V. N. Staroverov and G. E. Scuseria, Climbing the density functional ladder: Nonempirical meta-generalized gradient approximation designed for molecules and solids, *Phys. Rev. Lett.*, 2003, **91**, 146401.

8 A. Schäfer, H. Horn and R. Ahlrichs, Fully optimized contracted Gaussian basis sets for atoms Li to Kr, *J. Chem. Phys.*, 1992, **97**, 2571–2577.

9 K. Eichkorn, F. Weigend, O. Treutler and R. Ahlrichs, Auxiliary basis sets for main row atoms and transition metals and their use to approximate Coulomb potentials, *Theor. Chem. Acc.*, 1997, **97**, 119–124.

10 C. A. Singh and P. A. Kollman, An approach to computing electrostatic charges for molecules, *J. Comp. Chem.*, 1984, **5**, 129–45.

11 B. H. Besler, K. M. Merz Jr. and P. A. Kollman, Atomic charges derived from semiempirical methods, *J. Comp. Chem.*, 1990, **11**, 431–439.

12 E. Sigfridsson and U. Ryde, A comparison of methods for deriving atomic charges from the electrostatic potential and moments, *J. Comp. Chem.*, 1998, **19**, 377–395.

13 D. Case, H. Aktulga, K. Belfon, I. Ben-Shalom, J. Berryman, S. Brozell, D. Cerutti, T. Cheatham III, G. Cisneros, V. Cruzeiro, T. Darden, R. Duke, G. Giambasu, M. Gilson, H. Gohlke, A. Goetz, R. Harris, S. Izadi, S. Izmailov, K. Kasavajhala, M. Kaymak, E. King, A. Kovalenko, T. Kurtzman, T. Lee, S. LeGrand, P. Li, C. Lin, J. Liu, T. Luchko, R. Luo, M. Machado, V. Man, M. Manathunga, K. Merz, Y. Miao, O. Mikhailovskii, G. Monard, H. Nguyen, K. O'Hearn, A. Onufriev, F. Pan, S. Pantano, R. Qi, A. Rahnamoun, D. Roe, A. Roitberg, C. Sagui, S. Schott-Verdugo, A. Shajan, J. Shen, C. Simmerling, N. Skrynnikov, J. Smith, J. Swails, R. Walker, J. Wang, J. Wang, H. Wei, R. Wolf, X. Wu, Y. Xiong, Y. Xue, D. York, S. Zhao and P. Kollman, *AMBER 2022*, 2022, University of California, San Francisco.

14 L. Hu, P. Söderhjelm and U. Ryde, On the Convergence of QM/MM Energies, *J. Chem. Theory Comput.*, 2011, **7**, 761–777.

15 L. Hu, P. Söderhjelm and U. Ryde, Accurate Reaction Energies in Proteins Obtained by Combining QM/MM and Large QM Calculations, *J. Chem. Theory Comput.*, 2013, **9**, 640–649.

16 M. M. Hagemann, E. K. Wieduwilt, U. Ryde and E. D. Hedegård, Investigating the Substrate Oxidation Mechanism in Lytic Polysaccharide Monooxygenase: H2O2- versus O2-Activation, *Inorg. Chem.*, 2024, **63**, 21929–21940.

17 E. D. Hedegård and U. Ryde, Molecular mechanism of lytic polysaccharide monooxygenases, *Chem. Sci.*, 2018, **9**, 3866–3880.

18 M. M. Hagemann and E. D. Hedegård, Molecular Mechanism of Substrate Oxidation in Lytic Polysaccharide Monooxygenases: Insight from Theoretical Investigations, *Chem. Eur. J.*, 2023, **29**, e202202379.